

Fluid transients and fluid-structure interaction in flexible liquid-filled piping

Citation for published version (APA):

Wiggert, D. C., & Tijsseling, A. S. (2001). *Fluid transients and fluid-structure interaction in flexible liquid-filled piping*. (RANA : reports on applied and numerical analysis; Vol. 0117). Technische Universiteit Eindhoven.

Document status and date:

Published: 01/01/2001

Document Version:

Publisher's PDF, also known as Version of Record (includes final page, issue and volume numbers)

Please check the document version of this publication:

- A submitted manuscript is the version of the article upon submission and before peer-review. There can be important differences between the submitted version and the official published version of record. People interested in the research are advised to contact the author for the final version of the publication, or visit the DOI to the publisher's website.
- The final author version and the galley proof are versions of the publication after peer review.
- The final published version features the final layout of the paper including the volume, issue and page numbers.

[Link to publication](#)

General rights

Copyright and moral rights for the publications made accessible in the public portal are retained by the authors and/or other copyright owners and it is a condition of accessing publications that users recognise and abide by the legal requirements associated with these rights.

- Users may download and print one copy of any publication from the public portal for the purpose of private study or research.
- You may not further distribute the material or use it for any profit-making activity or commercial gain
- You may freely distribute the URL identifying the publication in the public portal.

If the publication is distributed under the terms of Article 25fa of the Dutch Copyright Act, indicated by the "Taverne" license above, please follow below link for the End User Agreement:

www.tue.nl/taverne

Take down policy

If you believe that this document breaches copyright please contact us at:

openaccess@tue.nl

providing details and we will investigate your claim.

RANA 01-17
May 2001

Fluid transients and fluid-structure interaction
in flexible liquid-filled piping

by

D.C. Wiggert and A.S. Tijsseling



Reports on Applied and Numerical Analysis
Department of Mathematics and Computing Science
Eindhoven University of Technology
P.O. Box 513
5600 MB Eindhoven, The Netherlands
ISSN: 0926-4507

FLUID TRANSIENTS AND FLUID-STRUCTURE INTERACTION IN FLEXIBLE LIQUID-FILLED PIPING

David C. Wiggert¹ and Arris S. Tijsseling²

ABSTRACT

Fluid-structure interaction in piping systems (FSI) consists of the transfer of momentum and forces between piping and the contained liquid during unsteady flow. Excitation mechanisms may be caused by rapid changes in flow and pressure or may be initiated by mechanical action of the piping. The interaction is manifested in pipe vibration and perturbations in velocity and pressure of the liquid. The resulting loads imparted on the piping are transferred to the support mechanisms such as hangers, thrust blocks, etc. The phenomenon has recently received increased attention because of safety and reliability concerns in power generation stations, environmental issues in pipeline delivery systems, and questions related to stringent industrial piping design performance guidelines. Furthermore, numerical advances have allowed practitioners to revisit the manner in which the interaction between piping and contained liquid is modeled, resulting in improved techniques that are now readily available to predict FSI. This review attempts to succinctly summarize the essential mechanisms that cause FSI, and present relevant data that describe the phenomenon. In addition, the various numerical and analytical methods that have been developed to successfully predict FSI will be described. Several earlier reviews regarding FSI in piping have been published; this review is intended to update the reader on developments that have taken place over the last approximately ten years, and to enhance the understanding of various aspects of FSI.

¹Dept. of Civil and Environmental Engineering, Michigan State University, East Lansing, MI 48824

²Dept. of Applied Mathematics and Computing Science, Eindhoven University of Technology, P.O. Box 513, 5600 MB Eindhoven, The Netherlands

TABLE OF CONTENTS

Nomenclature	3
1 Introduction	6
1.1 Description of FSI	6
2 Methods of analysis	8
2.1 Description of equation systems	8
2.1.1 Fluid transient	8
2.1.2 Piping structure	9
2.1.3 Applied fluid forces	11
2.2 Numerical solutions in the time domain	13
2.2.1 Method of characteristics	14
2.2.2 Finite element method	16
2.2.3 Simplified lumped structural parameter method	17
2.3 Analytical solutions in the frequency domain	18
2.4 Coupled versus uncoupled analysis	18
3 Transient FSI	20
3.1 Single straight pipe with valve excitation	20
3.2 Articulated pipe with valve excitation	21
3.3 Moving water-filled pipe with column separation	21
4 Periodic FSI	23
4.1 Single pipe including one elbow with valve excitation	23
4.2 Branch piping with valve excitation	23
5 Verification of the standard FSI model	25
5.1 Laboratory measurements	25
5.2 Field measurements	27
5.3 Numerical and parametric studies	28
6 Industrial applications of the standard FSI model	31
6.1 Anchor and support forces	31
6.2 Noise reduction	31
6.3 Vibration damping	32
6.4 Earthquake engineering	33
7 Extension of the standard FSI model	35
7.1 Non-elastic pipe wall material	35
7.2 Centrifugal and Coriolis forces	36
7.3 Distributed axial-lateral coupling	39
7.4 Curved pipes	39
7.5 Damping and friction	41
7.6 Cavitation	41
7.7 Alternative numerical methods	42
8 Conclusion	43
References (1-123)	44
Figures (1-22)	51
Tables (1-2)	79

NOMENCLATURE

Scalars

A	cross-sectional area, m^2
c	classical wave speed, celerity, m/s
\tilde{c}	FSI wave speed, celerity, m/s
D	inner diameter of pipe, m
E	Young modulus of pipe wall material, Pa
e	pipe wall thickness, m
f	frequency, $1/s$
FEM	Finite Element Method
FSI	Fluid-Structure Interaction
G	shear modulus of pipe wall material, Pa
H	pressure head, m
I	second moment of area, m^4
J	polar second moment of area, m^4
K	fluid bulk modulus, Pa
K^*	effective bulk modulus, Pa
k	spring stiffness, N/m
k_p	flexibility factor
L	length, m
l	wavelength, m
M	bending moment, Nm
MOC	Method of Characteristics
ODE	Ordinary Differential Equation(s)
P	pressure, Pa
PDE	Partial Differential Equation(s)
Q	shear force, N
R	inner radius of pipe, m
R_c	radius of curvature, m
T	period, s
t	time, s
u	pipe displacement, m

\dot{u}	pipe velocity, m/s
V	cross-sectional averaged fluid velocity, m/s
\forall	cavity volume, m ³
z	axial coordinate, m
α	change in flow direction, rad
γ	constant, m/s
ε	strain
θ	pipe rotation, rad
$\dot{\theta}$	rotational velocity of pipe, rad/s
κ^2	shear coefficient of pipe wall material
λ	bend ovalization parameter
ν	Poisson ratio
ρ	mass density, kg/m ³
σ	normal stress, Pa
ψ	bend pressurization parameter

Matrices and Vectors

F	generalized force vector
K	stiffness matrix
M	mass matrix
u	generalized displacement vector

Subscripts

<i>abs</i>	absolute
<i>b</i>	bending
<i>f, F</i>	fluid
<i>s</i>	shear
<i>t</i>	tube; axial (wave speed)
<i>tor</i>	torsion
<i>vapor</i>	vapor
<i>x</i>	lateral direction
<i>y</i>	lateral direction

z	axial direction
φ	hoop, circumferential direction
0	steady state

1 INTRODUCTION

This review deals with unsteady flows in liquid-filled, compliant piping systems. The phenomenon of pipe movement related to unsteady fluid motion is termed fluid-structure interaction, or simply FSI, an acronym that will be used throughout the paper. We restrict ourselves to piping completely filled with liquid, with the exception of occasional column separation conditions. Both transient and periodic flows will be considered, although more emphasis will be placed upon slightly-compressible (elastic) transient flow conditions, i.e., waterhammer. Between 1970 and 1980 a substantial amount of research activity focused on understanding and quantifying the mechanical interaction between unsteady flow in piping and the resulting vibration of the piping structure. Probably the most significant motivation for this endeavor came from the nuclear power industry, where a number of waterhammer incidents and resulting pipe motion occurred. Over the past ten years FSI has experienced renewed attention because of safety and reliability concerns in power generation stations, environmental issues in pipeline delivery systems, and questions related to stringent industrial piping design performance guidelines. Recent numerical advances have allowed practitioners to revisit the manner in which the interaction between piping and contained liquid is modeled, resulting in improved techniques that are now readily available to predict FSI.

The objectives of this paper are threefold: 1) succinctly summarize the essential mechanisms that cause FSI and present relevant data that demonstrate the phenomenon; 2) describe the various numerical and analytical methods that have been developed to successfully predict FSI; and 3) relate recent contributions in the field, with primary emphasis on those published since 1990. Exhaustive reviews by Tijsseling [1] and Wiggert [2,3] form the starting point for the present paper. Some studies published earlier than 1990 are included, since either they were not referenced in the earlier reviews or they provide continuity to this presentation.

1.1 Description of FSI

Fluid-structure interaction in piping systems consists of the transfer of momentum and forces between piping and the contained liquid during unsteady flow. Excitation mechanisms may be caused by rapid changes in flow and pressure or may be initiated by mechanical action of the piping. The interaction is manifested in pipe vibration and perturbations in velocity and pressure of the liquid. The resulting loads imparted on the piping are transferred to the support

mechanisms such as hangers, thrust blocks, etc.

Three coupling mechanisms can be identified in FSI: Poisson coupling, friction coupling and junction coupling. *Poisson coupling* is associated with the circumferential (hoop) stress perturbations produced by liquid pressure transients that translate to axial stress perturbations by virtue of the Poisson ratio coefficient. The axial stress and accompanying axial strain perturbations travel as waves in the pipe wall at approximately the speed of sound in solid beams. Typically its magnitude is three to five times greater than the acoustic velocity in the contained liquid in the pipe. *Friction coupling* is created by the transient liquid shear stresses acting on the pipe wall; usually it is insignificant when compared to the other two coupling mechanisms. Both Poisson and friction coupling are distributed along the axis of a pipe element. The third, and often the most significant, coupling mechanism is *junction coupling*, which results from the reactions set up by unbalanced pressure forces and by changes in liquid momentum at discrete locations in the piping such as bends, tees, valves, and orifices. Sources of excitation include not only those associated with liquid motion, but also from the structural side, see Figure 1. In flexible piping, waterhammer waves impacting at junctions may set up vibrations that in turn may translate to a variety of structural responses (bending, torsion, shear, axial stresses) at locations distant from the junction. In addition, the vibrating junction will induce fluid transients in the contained liquid column, with acoustic waves traveling away from the junction. The result will be complex interactive motions in both the piping and liquid, with subsequent waveforms highly dependent on the geometry of the piping structure.

In Section 2 we present the equations of a so-called “standard model,” one that defines FSI in a form suitable for waterhammer in piping systems. Methods of solution using the standard model for elementary piping systems are found in Sections 3 and 4; in the former, numerical solutions are in the time domain, and in the latter, analytical solutions are in the frequency domain. The remaining sections deal primarily with verification, application and extension of the standard model.

2 METHODS OF ANALYSIS

2.1 Description of equation systems

The one-dimensional model presented consists of 14 first-order partial differential equations or, alternatively, 4 higher-order equations. It is valid for the low-frequency acoustic behavior of straight, thin-walled, linearly elastic, prismatic pipes of circular cross-section containing a weakly compressible (elastic) liquid. This means that V/c , e/R , D/l and P/K (the symbols are defined in the Nomenclature) are small with respect to unity. Axial, lateral and torsional vibrations are assumed not to influence each other along a straight pipe. In the axial vibration a dynamic liquid-pipe (Poisson) coupling exists, whereas in the lateral vibration the contained liquid acts as added mass. Torsional vibration is assumed not to be affected by the liquid. The effects of damping, friction and gravity (e.g., falling pipe) are ignored herein.

The assumed radial pipe motion is quasi-static, because inertia forces in the radial direction are neglected in both the liquid and the pipe wall. The hoop stress is then linearly related to the pressure by

$$\sigma_{\varphi} = \frac{R}{e} P \quad (2.1)$$

Equation 2.1, which probably is the oldest FSI formula, is implicitly included in the relations governing axial liquid-pipe motion. In multi-pipe systems, the vibrations of the individual pipes are coupled at junctions. Junction coupling is modeled through local continuity and equilibrium principles.

2.1.1 Fluid transient

The extended waterhammer equations

$$\frac{\partial V}{\partial t} + \frac{1}{\rho_f} \frac{\partial P}{\partial z} = 0 \quad (2.2)$$

$$\frac{\partial V}{\partial z} + \left\{ \frac{1}{K} + (1 - \nu^2) \frac{2R}{Ee} \right\} \frac{\partial P}{\partial t} = 2\nu \frac{\partial \dot{u}_z}{\partial z} \quad (2.3)$$

govern the unknowns of fluid pressure, P , cross-sectional averaged fluid velocity, V , and axial pipe velocity, \dot{u}_z . The pressures and velocities are mean values for the cross sections. Equations 2.2 and 2.3 describe the propagation of pressure waves under the influence of axial pipe vibrations. The classical waterhammer equations are obtained for the hypothetical case $\nu = 0$.

The wave equation—in terms of P —corresponding to Eqs. 2.2 and 2.3 is

$$\frac{\partial^2 P}{\partial t^2} - \frac{K^*}{\rho_f} \frac{\partial^2 P}{\partial z^2} = 2\nu K^* \frac{\partial^3 u_z}{\partial t^2 \partial z} \quad (2.4)$$

where u_z is the axial pipe displacement and

$$\frac{1}{K^*} = \frac{1}{K} + (1 - \nu^2) \frac{2R}{Ee} \quad (2.5)$$

2.1.2 Piping structure

Axial motion. The extended beam equations

$$\frac{\partial \dot{u}_z}{\partial t} - \frac{1}{\rho_t} \frac{\partial \sigma_z}{\partial z} = 0 \quad (2.6)$$

$$\frac{\partial \dot{u}_z}{\partial z} - \frac{1}{E} \frac{\partial \sigma_z}{\partial t} = - \frac{\nu R}{Ee} \frac{\partial P}{\partial t} \quad (2.7)$$

govern the unknowns of axial pipe stress, σ_z , axial pipe velocity, \dot{u}_z , and fluid pressure, P . Equations 2.6 and 2.7 describe the propagation of axial stress waves under the influence of pressure variation in the fluid. The classical beam equations are obtained for the hypothetical case $\nu = 0$.

The wave equation—in terms of u_z —corresponding to Eqs. 2.6 and 2.7 is

$$\frac{\partial^2 u_z}{\partial t^2} - \frac{E}{\rho_t} \frac{\partial^2 u_z}{\partial z^2} = \frac{\nu R}{\rho_t e} \frac{\partial P}{\partial z} \quad (2.8)$$

Lateral motion. The Timoshenko beam equations

$$\frac{\partial \dot{u}_y}{\partial t} + \frac{1}{e_t A_t + e_f A_f} \frac{\partial Q_y}{\partial z} = 0 \quad (2.9)$$

$$\frac{\partial \dot{u}_y}{\partial z} + \frac{1}{\kappa^2 G A_t} \frac{\partial Q_y}{\partial t} = - \dot{\theta}_x \quad (2.10)$$

$$\frac{\partial \dot{\theta}_x}{\partial t} + \frac{1}{e_t I_t} \frac{\partial M_x}{\partial z} = \frac{1}{e_t I_t} Q_y \quad (2.11)$$

$$\frac{\partial \dot{\theta}_x}{\partial z} + \frac{1}{E I_t} \frac{\partial M_x}{\partial t} = 0 \quad (2.12)$$

govern the unknowns of lateral shear force, Q_y , lateral pipe velocity, \dot{u}_y , bending moment, M_x , and rotational pipe velocity $\dot{\theta}_x$. The shear coefficient $\kappa^2 = 2(1 + \nu)/(4 + 3\nu)$ according to Cowper [4]. Equations 2.9 to 2.12 describe flexural (shear and bending) vibration in the y - z plane. A similar set of equations describes lateral vibration in the x - z plane. Coriolis and centrifugal forces induced by high flow velocities are disregarded. The equations for a Bernoulli-Euler beam are obtained when shear deformation (second term in Eq. 2.10) and rotational inertia (first term in Eq. 2.11) are neglected.

The conventional beam equation—in terms of u_y —corresponding to Eqs. 2.9 - 2.12 is

$$\begin{aligned} & (e_t A_t + e_f A_f) \frac{\partial^2 u_y}{\partial t^2} + E I_t \frac{\partial^4 u_y}{\partial z^4} + \\ & - E I_t \frac{e_t A_t + e_f A_f}{\kappa^2 G A_t} \frac{\partial^4 u_y}{\partial t^2 \partial z^2} - e_t I_t \frac{\partial^4 u_y}{\partial t^2 \partial z^2} + e_t I_t \frac{e_t A_t + e_f A_f}{\kappa^2 G A_t} \frac{\partial^4 u_y}{\partial t^4} = 0 \end{aligned} \quad (2.13)$$

The first two terms represent the classical Bernoulli-Euler beam, the third and fourth terms are due to shear deformation and rotational inertia, respectively, and the last term appears when both shear deformation and rotational inertia are modeled.

Torsional motion. The torsional equations

$$\frac{\partial \dot{\theta}_z}{\partial t} - \frac{1}{\rho_t J_t} \frac{\partial M_z}{\partial z} = 0 \quad (2.14)$$

$$\frac{\partial \dot{\theta}_z}{\partial z} - \frac{1}{G J_t} \frac{\partial M_z}{\partial t} = 0 \quad (2.15)$$

govern the unknowns of torsional moment, M_z , and torsional angular velocity, $\dot{\theta}_z$. Equations 2.14 and 2.15 describe torsional vibration around the central (z -) axis of the pipe.

The wave equation—in terms of θ_z —corresponding to Eqs. 2.14 and 2.15 is

$$\frac{\partial^2 \theta_z}{\partial t^2} - \frac{G}{\rho_t} \frac{\partial^2 \theta_z}{\partial z^2} = 0 \quad (2.16)$$

2.1.3 Applied fluid forces

The fluid exerts forces on the pipes, and vice versa, through the friction, Poisson and junction coupling mechanisms described in Section 1.1. Being relatively weak, friction coupling is not considered herein and Poisson coupling is modeled through the right-hand sides of Eq. 2.3 or 2.4, and Eq. 2.7 or 2.8. Junction coupling is a local event, which is modeled through boundary and junction conditions. Four examples are given below.

Closed end. Pipes may experience severe fluid forces at dead ends, recognizing that pressure waves double in magnitude upon reflection at immovable closed ends. For movable (and massless) closed ends strong FSI may occur, according to the following relations:

$$V = \dot{u}_z \quad \text{and} \quad A_f P = A_t \sigma_z \quad (2.17)$$

Miter bend. Movable bends are the most likely origin of FSI in industrial systems. The in-plane vibration of a bend couples fluid and pipe variables:

$$\{ A_f (V - \dot{u}_z) \}_1 = \{ A_f (V - \dot{u}_z) \}_2 \quad \text{and} \quad \{ P \}_1 = \{ P \}_2 \quad (2.18a)$$

$$\begin{aligned} \{ \dot{u}_z \}_1 &= \{ \dot{u}_z \}_2 \cos \alpha + \{ \dot{u}_y \}_2 \sin \alpha \quad \text{and} \\ \{ A_f P - A_t \sigma_z \}_1 &= \{ A_f P - A_t \sigma_z \}_2 \cos \alpha + \{ Q_y \}_2 \sin \alpha \end{aligned} \quad (2.18b)$$

$$\begin{aligned} \{ \dot{u}_y \}_1 &= \{ \dot{u}_y \}_2 \cos \alpha - \{ \dot{u}_z \}_2 \sin \alpha \quad \text{and} \\ \{ Q_y \}_1 &= \{ Q_y \}_2 \cos \alpha - \{ A_f P - A_t \sigma_z \}_2 \sin \alpha \end{aligned} \quad (2.18c)$$

$$\{ \dot{\theta}_x \}_1 = \{ \dot{\theta}_x \}_2 \quad \text{and} \quad \{ M_x \}_1 = \{ M_x \}_2 \quad (2.18d)$$

where α is the change in flow direction and the indices 1 and 2 refer to either side of the bend. The mass and dimensions of the bend are neglected, as are the forces due to change in liquid momentum, which is consistent with the acoustic approximation. This simple model is valid if the length of the elbow is small compared to the lengths of the adjacent pipes. The angle $\pi - \alpha$ between the pipes remains constant; elbow ovalization and the associated flexibility increase and stress intensification are ignored. However, these effects can be accounted for by flexibility and stress-intensification factors. The special case $\alpha = 0$ describes a diameter change (sudden pipe expansion/contraction). The out-of-plane vibration of the bend, which is decoupled from its in-plane vibration, has no FSI mechanisms.

T-section. The transmission and reflection of pressure and stress waves at unrestrained T-shaped pipe branches involve in-plane liquid-pipe coupling according to:

$$\begin{aligned} \{ A_f (V - \dot{u}_z) \}_1 &= \{ A_f (V - \dot{u}_z) \}_2 + \{ A_f (V - \dot{u}_z) \}_3 \quad \text{and} \\ \{ P \}_1 &= \{ P \}_2 = \{ P \}_3 \end{aligned} \quad (2.19a)$$

$$\begin{aligned} \{ \dot{u}_z \}_1 &= \{ \dot{u}_y \}_2 = \{ -\dot{u}_y \}_3 & \text{and} \\ \{ A_f P - A_t \sigma_z \}_1 &= \{ Q_y \}_2 - \{ Q_y \}_3 \end{aligned} \quad (2.19b)$$

$$\begin{aligned} \{ \dot{u}_y \}_1 &= \{ -\dot{u}_z \}_2 = \{ \dot{u}_z \}_3 & \text{and} \\ \{ -Q_y \}_1 &= \{ A_f P - A_t \sigma_z \}_2 - \{ A_f P - A_t \sigma_z \}_3 \end{aligned} \quad (2.19c)$$

$$\begin{aligned} \{ \dot{\theta}_x \}_1 &= \{ \dot{\theta}_x \}_2 = \{ \dot{\theta}_x \}_3 & \text{and} \\ \{ M_x \}_1 &= \{ M_x \}_2 + \{ M_x \}_3 \end{aligned} \quad (2.19d)$$

where the indices 1, 2 and 3 refer to the three sides of the T-piece. The mass and dimensions of the T-piece are neglected, as are the forces due to changes in liquid momentum, which is consistent with the acoustic approximation. The angles between the pipes are assumed to remain at 90 degrees. The out-of-plane vibration of the T-section, which is decoupled from its in-plane vibration, has no FSI mechanisms.

Column separation. Dangerous fluid forces may be created when liquid columns are ruptured due to ambient pressures nearly reaching vapor conditions and subsequently collapsed due to inertial forces acting on the surrounding liquid column(s). The mechanism is that of a high-speed liquid column impacting with a closed end or an adjacent liquid column, resulting in severe pipe transients. For an unsupported dead end, the equations describing the growth and collapse of a column separation are:

$$P_{abs} = P_{vapor}, \quad \frac{\partial \mathcal{V}}{\partial t} = \pm A_f (V - \dot{u}_z) \quad \text{and} \quad A_f P = A_t \sigma_z \quad (2.20)$$

where the void has volume, \mathcal{V} , and absolute pressure, P_{abs} . The latter is held equal to the vapor pressure, P_{vapor} . The \pm sign indicates dependency on the direction of the z -coordinate.

2.2 Numerical solutions in the time domain

The basic equations and boundary (and initial) conditions presented in Section 2.1 can be numerically solved in many ways. In the time domain, the fluid equations are often solved by

the method of characteristics (MOC) and the structural equations by the finite element method (FEM). For fluid-structural coupled problems it is advantageous to use *one* method for all equations. In this section we show how all equations can be solved with either MOC or FEM. Additionally, a simplified method based on lumped structural parameters is given.

Numerous investigators have successfully applied hybrid (MOC-FEM) methods as well as finite difference methods; some of these will be discussed in subsequent sections.

2.2.1 Method of characteristics

The ten first-order partial differential equations (PDE) presented in Section 2.1 are solved by the MOC. In practice, fourteen equations are to be solved, because of a second set of lateral relations analogous to Eqs. 2.9 - 2.12. The MOC transforms the PDE to ODE (ordinary differential equations), which are valid, and integrated, along characteristic lines in the distance-time plane. A time-marching procedure gives the desired solution.

Axial motion. The MOC transforms the coupled Eqs. 2.2, 2.3, 2.6, and 2.7 into the following so-called compatibility equations:

$$\frac{dV}{dt} \pm \frac{1}{\rho_f \tilde{c}_F} \frac{dP}{dt} + 2\nu \frac{(\tilde{c}_F / c_t)^2}{1 - (\tilde{c}_F / c_t)^2} \frac{d\dot{u}_z}{dt} \mp \frac{2\nu}{\rho_t \tilde{c}_F} \frac{(\tilde{c}_F / c_t)^2}{1 - (\tilde{c}_F / c_t)^2} \frac{d\sigma_z}{dt} = 0 \quad (2.21)$$

$$\frac{d\dot{u}_z}{dt} \mp \frac{1}{\rho_t \tilde{c}_t} \frac{d\sigma_z}{dt} - \nu \frac{R}{e} \frac{\rho_f}{\rho_t} \frac{(c_F / \tilde{c}_t)^2}{1 - (c_F / \tilde{c}_t)^2} \frac{dV}{dt} \mp \nu \frac{R}{e} \frac{1}{\rho_t \tilde{c}_t} \frac{(c_F / \tilde{c}_t)^2}{1 - (c_F / \tilde{c}_t)^2} \frac{dP}{dt} = 0 \quad (2.22)$$

which are valid along the characteristic lines defined by

$$\frac{dz}{dt} = \pm \tilde{c}_F \quad \text{and} \quad \frac{dz}{dt} = \pm \tilde{c}_t \quad (2.23)$$

respectively.

The classical pressure and stress wave speeds

$$c_F = \left\{ \frac{K^*}{\varrho_f} \right\}^{1/2} \quad \text{and} \quad c_t = \left\{ \frac{E}{\varrho_t} \right\}^{1/2} \quad (2.24)$$

differ slightly from the actual (with FSI) wave speeds

$$\begin{aligned} \tilde{c}_F &= \frac{1}{2} \sqrt{2} \left\{ \gamma^2 - (\gamma^4 - 4 c_F^2 c_t^2)^{1/2} \right\}^{1/2} \quad \text{and} \\ \tilde{c}_t &= \frac{1}{2} \sqrt{2} \left\{ \gamma^2 + (\gamma^4 - 4 c_F^2 c_t^2)^{1/2} \right\}^{1/2} \end{aligned} \quad (2.25)$$

where

$$\gamma^2 = \left(1 + 2 \nu^2 \frac{\varrho_f}{\varrho_t} \frac{R}{e} \right) c_F^2 + c_t^2$$

It is noted that $\tilde{c}_F \tilde{c}_t = c_F c_t$.

Equations 2.21 - 2.23 can be integrated exactly.

Lateral motion. First, note that the MOC does not apply when considering a Bernoulli-Euler beam. The compatibility relations belonging to the Timoshenko set, Eqs. 2.9 - 2.12, are:

$$\frac{d \dot{u}_y}{d t} \pm \frac{c_s}{\kappa^2 G A_t} \frac{d Q_y}{d t} = \mp c_s \dot{\theta}_x \quad (2.26)$$

$$\frac{d \dot{\theta}_x}{d t} \pm \frac{c_b}{E I_t} \frac{d M_x}{d t} = \frac{1}{\varrho_t I_t} Q_y \quad (2.27)$$

These are valid along the characteristic lines defined by

$$\frac{d z}{d t} = \pm c_s \quad \text{and} \quad \frac{d z}{d t} = \pm c_b \quad (2.28)$$

respectively.

The classical shear and bending wave speeds are

$$c_s = \left\{ \frac{\kappa^2 G A_t}{\rho_t A_t + \rho_f A_f} \right\}^{1/2} \quad \text{and} \quad c_b = \left\{ \frac{E}{\rho_t} \right\}^{1/2} \quad (2.29)$$

Equations 2.26 and 2.27 are integrated numerically.

Torsional motion. The compatibility relations pertaining to Eqs. 2.14 and 2.15 are

$$\frac{d \dot{\theta}_z}{d t} \mp \frac{c_{tor}}{G J_t} \frac{d M_z}{d t} = 0 \quad (2.30)$$

The corresponding characteristic lines follow from

$$\frac{d z}{d t} = \pm c_{tor} \quad (2.31)$$

where

$$c_{tor} = \left\{ \frac{G}{\rho_t} \right\}^{1/2} \quad (2.32)$$

Equations 2.30 and 2.31 can be integrated exactly.

2.2.2 Finite element method

The FEM is a powerful and well-documented numerical procedure for solving problems in engineering mechanics. The application of the FEM to the basic equations of Section 2.1 is straightforward, provided that the FSI coupling conditions of Section 2.1.3 are carefully taken into account. A general outline of the method is given herein.

In structural dynamics the FEM is formulated in terms of the unknown displacement, u , which is a continuous function. The piping structure is therefore modeled by the higher-order equations Eq. 2.8, Eq. 2.13 (twice) and Eq. 2.16 describing axial, lateral—in two perpendicular directions—and torsional motion, respectively. The fluid is modeled through Eq. 2.4 in terms of

the unknown pressure, P , which is assumed to be continuous at pipe junctions. The general procedure is to take weak (virtual work) formulations of the basic equations and integrate these by parts to reduce the order of the spatial derivatives of u . Shape and test functions are defined in agreement with static pipe deformations. So-called element mass and stiffness matrices, valid for one pipe section, are obtained. The piping structure is divided into sections and the corresponding element matrices are assembled into global matrices representing the entire system. The final result is a linear system of ODE:

$$\mathbf{M}\ddot{\mathbf{u}} + \mathbf{K}\mathbf{u} = \mathbf{F}(t) \quad (2.33)$$

where \mathbf{M} is the mass matrix, \mathbf{K} is the stiffness matrix, \mathbf{F} is the load vector, and \mathbf{u} the displacement vector. Boundary and junction conditions are incorporated in Eq. 2.33 and all quantities are taken relative to a global coordinate system. In the modal analysis approach, the system of coupled equations represented by Eq. 2.33 is diagonalized. To do so, the system's eigen-values (frequencies) and eigen-vectors (modes) have to be calculated. The resulting decoupled ODE are treated as single-degree-of-freedom systems. In the direct time-integration approach, Eq. 2.33 is integrated numerically using Wilson- θ , Newmark- β or Hilber-Hughes-Taylor- α [Hilber et al, 5] schemes.

2.2.3 Simplified lumped structural parameter method

FSI in piping systems is caused by *axial* motions of liquid and pipe. The four-equation model described by Eqs. 2.2, 2.3, 2.6 and 2.7 is sufficient to describe coupled axial motion. Interaction with lateral motion takes place at bends and branches only. Wiggert et al [6] modeled pipe flexure quasi-statically by springs placed at elbows. This approach greatly simplifies the computational procedure, because the lateral relations (Eqs. 2.9 - 2.12) and the torsional relations (Eqs. 2.14 and 2.15) are disregarded. It gave excellent results for their two-elbow planar test circuit.

Miter bend. Equations 2.18a, 2.18b, and 2.18c are applied with

$$\{ Q_y \}_1 = - \{ k_y u_y \}_1 \quad \text{and} \quad \{ Q_y \}_2 = \{ k_y u_y \}_2 \quad (2.34)$$

where k_y is the flexural spring stiffness. For example, $k_y = 3 E I_t / L^3$ with L the distance between the elbow and its nearest rigid support. Note that the vibration of an L-shaped system rigidly supported at its ends is dominated by axial stiffness, so that k_y can satisfactorily be ignored.

2.3 Analytical solutions in the frequency domain

Where time-domain solutions are the preferred option for transient events, frequency-domain solutions are best to describe free and forced vibrations. Harmonic, Fourier and Laplace analyses replace the time variable in the governing PDE by a frequency parameter. The resulting ODE can be integrated exactly.

For example, the Laplace transform applied to the first-order equations in Section 2.1 replaces all time derivatives of a variable by s multiplied with the Laplace transform of that variable, where $s = i\omega$ is the complex frequency. The obtained linear system of first-order ODE for the Laplace-transformed variables can be integrated exactly. The solution, which depends on frequency, is conveniently formulated in terms of transfer matrices that relate state vectors at different positions. Alternatively, impedance matrices or dynamic stiffness matrices can be defined. The transfer matrices of all pipes in the system, together with boundary and junction conditions, are assembled in one global matrix. Sources of pulsation (fluid) and vibration (structure) are placed in the excitation vector. Repeat calculations for a range of frequencies finally give desired information such as resonance frequencies, mode shapes, power spectra, etc.

Of course, the Laplace transform can be applied to the higher-order equations in Section 2.1, or, importantly, to the FEM formulation, Eq. 2.33. For axial and torsional motion, the transfer matrices can be obtained directly from MOC transformation matrices [Zhang et al, 7, 35].

2.4 Coupled versus uncoupled analysis

The classical waterhammer problem consists of a reservoir-pipe-valve system subjected to instantaneous valve closure. The classical frictionless solution for the dynamic pressure at the valve is a repeating square wave. In this solution, the infinite-medium wave speed is lowered by the hoop elasticity of the pipe wall, but any other pipe effects are neglected. One classical FSI problem consists of the same system, but now with axial pipe motion generated by vibration of the valve. The influence of pipe motion on waterhammer pressures is clearly seen from the Figures 2 and 3. The test system is a 20-m-long steel pipe filled with water. The pipe diameter is

0.8 m and the wall thickness is 8 mm. Figure 2 (top) shows calculated pressure histories at the valve. The instantaneous valve closure produces a square wave for classical waterhammer and multiple square waves when FSI is taken into account. The influence of axial stress waves, traveling five times faster than pressure waves, is evident. In all cases, they lead to larger extreme pressures. Figure 2 (bottom) of the valve displacement shows a general trend: uncoupled calculations may exhibit resonance, where the more realistic coupled calculations do not. Figure 3 (bottom) shows calculated pressures in the frequency domain. FSI changes the classical waterhammer frequency spectrum, primarily around the natural frequencies of the axial pipe vibration. In fact, FSI tends to separate coinciding fluid and pipe natural frequencies, thereby preventing resonance behavior of the type shown in Figure 2 (bottom). Hara [8, Fig. 7b] and Diesselhorst et al [9, Fig. 7] give good examples of this phenomenon.

3 TRANSIENT FSI

The theory presented in Section 2 has been validated against experimental data by numerous researchers. Many of them are referred to in earlier review papers [Tijsseling 1; Wiggert, 2,3]. Recent work is discussed in Section 5. Some typical results obtained for transient vibration are given here. Periodic vibration is considered in Section 4.

3.1 Single straight pipe with valve excitation

Budny [10] investigated the dynamic behavior of a single pipe subjected to waterhammer loads. His laboratory apparatus consisted of a 47.7 meters long hydraulic system leading water from an upstream reservoir to a downstream valve. It included a 22.1 meters long test section extending from the axially unrestrained valve to a rigid anchor upstream. Rapid valve closure caused significant structural motion of the wire-suspended test pipe. The copper pipe had an internal diameter of 26 mm and 1.3 mm thick walls.

Figure 4 shows typical results for the dynamic pressure at the valve. The broken line is the classical waterhammer square wave that is valid for instantaneous valve closure in an axially immovable (and frictionless) pipe. The wave amplitude, ΔP , is proportional to the initial flow velocity, V_0 , according to the Joukowsky formula

$$\Delta P = \rho_f c_F V_0 \quad (3.1)$$

and the wave period, T , is $4L/c_F$ for an open-closed system. Here, the classical pressure wave speed, c_F , is 1288 m/s (Eq. 2.24). The square wave is the exact solution of the conventional waterhammer relations, Eqs. 2.2 and 2.3, under the assumption of zero (or constant) axial pipe strain ($\varepsilon_z = \partial u_z / \partial z$). If transient axial strains are taken into account, the two pipe equations, Eqs. 2.6 and 2.7, come into play. The solid line is the numerical solution to the four FSI relations, Eqs. 2.2, 2.3, 2.6 and 2.7, combined with the boundary condition at the valve, Eqs. 2.17. The pressure wave speed is slightly changed: \tilde{c}_F is 1263 m/s (Eq. 2.25). The axial vibration of the pipe produces a higher-frequency fluctuation on top of the square pressure wave, mainly due to pumping action of the closed end. Two general trends are visible: wave fronts become less steep and attenuated as time advances and the dynamic pressure exceeds the value predicted by the Joukowsky Eq. 3.1. Budny's experiment (dotted line) confirms the FSI theory.

3.2 Articulated pipe with valve excitation

Dynamic pressures exceeding the Joukowsky limit given by Eq. 3.1 and wave attenuation are even more evident in the large-scale experiment of Kruisbrink and Heinsbroek [11,12]. The test system shown in Figure 5 consists of seven straight pipe sections connected by 90-degree miter bends. The total length of the hydraulic system is 77.5 m, including 1.5 m of pipe between fixed point A and the reservoir. The wire-suspended steel pipes have an internal diameter of 109 mm, are 3 mm thick and convey water. The structural system is highly flexible and easily excited by closure of the fast-acting valve at fixed point H. The bends C, D, E and F are virtually unsupported; the bends B and G are restrained in lateral directions only. The results shown here were obtained without employing the adjustable spring at E.

The measured (solid line) and calculated (dashed line) pressure histories at the valve in Figure 6a are entirely different from the classical waterhammer square wave (dotted line). It is worthy to note that the fundamental frequency, $c_f/(4L)$, of the classical wave is 4 Hz, which would be valid for a very rigid system, whereas the actual frequency is 5 Hz. Someone not aware of the effects of FSI might conclude from this latter frequency that the pressure wave speed, c_f , is 1550 m/s, a value higher than the speed of sound in unconfined water. The fundamental frequency of 5 Hz, the trident shape just after valve closure, the attenuation of the square wave and the pressure amplitudes are well predicted by the numerical calculation. For impact-loaded flexible systems like the one considered, a fully coupled computation is prerequisite. The same test rig data modeled by Kruisbrink and Heinsbroek was analyzed by Enkel and Grams [13] using a modal analysis technique for the piping structure; their predicted results were similar to the Delft results, Fig. 6b.

3.3 Moving water-filled pipe with column separation

Tijsseling and Fan [14] used a single closed pipe to validate the FSI column-separation model given by Eqs. 2.20. The wire-suspended steel pipe was internally pressurized with water and externally struck at one of its sealed ends by an in-line steel rod. Depending on the static pressure of the water and the impact velocity of the rod, transient column separation developed at the pipe ends. The 4.5-m-long pipe had an internal diameter of 52 mm and a wall thickness of 4 mm. Experimental and theoretical results for four different static pressures, P_0 , are displayed in Figure 7. The middle four graphs show measured (solid line) and calculated (broken line) absolute pressures at the non-impacted pipe end. The corresponding void volumes (calculated), which by definition are non-zero at vapor pressure ($P_{vapor} = 0$ MPa), are given in the top and bottom graphs.

Column separation does not occur in the time histories shown upper-left, because the static pressure in the system is high enough to prevent it. In that case the void volume remains zero and excellent agreement is found between measured and calculated pressures. Note that the dynamic pressures do not depend on the static pressure if column separation is absent. The other three pressure histories show clear evidence of column separation ($P = 0$ MPa). The agreement between theory and experiment is still excellent for the initial stage of the transient event, but becomes less similar when column separation forms repeatedly. This is due to regions of distributed cavitation along the pipe, something not accounted for in the numerical solutions shown.

The numerical results were obtained with the MOC and therefore based on the wave paths illustrated in Figure 8. The left diagram, showing the fronts of pressure and stress (precursor) waves in the distance-time plane, corresponds to the upper-left of Figure 7 (no column separation). The impact rod is in contact with the pipe for a time period $2L/c_t$ and each incident wave gives two reflected waves. The right diagram, corresponding to the bottom-right of Figure 7, reveals that the first column separation (thick vertical line) occurs at the far end and the second one at the impact end. After time $9L/c_t$, column separation at both ends exists simultaneously for a short period.

4 PERIODIC FSI

Lesmez [15], Tentarelli [16], Brown and Tentarelli [17], Tentarelli and Brown [18], Frikha [19], De Jong [20] and Svingen [21, 22] have studied FSI in pipe systems that were excited by periodic forces. They compared their theoretical solutions in the frequency domain with original data measured in the laboratory. Results obtained by Svingen and by Tentarelli are presented herein.

4.1 Single pipe including one elbow with valve excitation

Svingen [21, 22] built an L-shaped test system with an 8.5 m long vertical pipe, an 11.3 m long horizontal pipe and a short connecting bend (flexibility factor 10.7). The vertical pipe was fed with water from a tank at its top and the horizontal pipe discharged into open atmosphere through an 80 by 10-mm orifice. The system, supported at the upstream tank and near the downstream orifice only, was highly flexible because of the very thin-walled steel pipes used (1.5 mm wall thickness, 80 mm inner diameter). This high flexibility made FSI more significant at the expense of dead weight sagging of the horizontal pipe (up to 30 mm). Detailed dimensions of the test rig are given in Figure 9. A rotating disk interrupting the outflow excited the pipe system. Three disks were specially designed and manufactured with high precision to guarantee sinusoidal excitation of constant amplitude over a wide range of frequencies (up to 300 Hz). Svingen computed the dynamic response of the test system through application of the FEM in the frequency domain. Figure 10 shows frequency spectra for the pressure near the outflow. It is obvious that the classical waterhammer (no FSI) prediction in the left figure is inferior to the FSI prediction in the right figure: the latter corresponds much better to the experimental signal. To further improve that correspondence, damping was introduced in the calculation (right figure), in order to prevent infinitely high (anti-) resonance peaks.

4.2 Branch piping with valve excitation

Tentarelli [16], Brown and Tentarelli [17], Tentarelli and Brown [18], performed experiments in the relatively complex three-dimensional system shown in Figure 11. The system was made up of steel pipes (10-mm inner diameter, 1.2-mm wall thickness) and filled with hydraulic oil. It consisted of five straight sections of 4-m total length, one T-piece, one elbow, two bends, one free and one restrained closed end, and one restrained end exposed to pressure excitation. The whole system was clamped in a 150 kg vice, without further supports, suffering some dead-weight deformation. Figure 11 gives the amount of detail needed to accurately simulate the system. In particular, care had to be taken in modelling the fittings. For example, in one experiment Tentarelli

found that an elbow was better modelled by two short and thick sections of pipe than by a lumped mass. By taking care of these minor details, computed results were found to be excellent. Figure 12 shows the pressure at the free closed end, divided by the pressure excitation, as a function of frequency. The theoretical spectrum, based on numerically treated analytical solutions, and the experimental record are nearly identical. Minor deviations were attributed to measurement errors.

5 VERIFICATION OF THE STANDARD FSI MODEL

The standard FSI model, described by the equations and methods of solution presented in Section 2 is analyzed in Sections 3 and 4, and compared with several exhaustive experiments. In this section, additional verification and refinements to the standard model are presented, which further substantiate the FSI methodology. The verification includes both laboratory and field measurements.

5.1 Laboratory measurements

Time domain. A number of papers have dealt with the analysis of FSI in the time domain using the standard numerical or analytical methods. Most of the reported studies make use of laboratory-derived data for purposes of verification. In addition to the work of Budny [10] mentioned in Section 3.1, Wiggert et al [23] verified a method of characteristics solution for both the contained liquid and piping components using data from a piping system that exhibited two-degree-of-freedom motion [Wiggert et al, 6]. It was noted, however, that no significant shear and bending moments were present in the experiment, so that the numerical model was not severely tested in predicting those modes.

Heinsbroek and Kruisbrink [24] validated the hybrid numerical code FLUSTRIN developed by Delft Hydraulics Laboratory using a large-scale three-dimensional test rig, Figures 5 and 6. The code makes use of the method of characteristics to solve the fluid equations and finite elements for the Bernoulli-Euler based structural equations. These experimental data are probably the most comprehensive that have been collected for studying FSI in a compliant piping system where junction coupling plays a dominant role. The predictions show excellent correlation with the data, including fluid pressures, structural displacements, and strains—a total of seventy recorded signals (Heinsbroek and Kruisbrink [25]). In related studies, Heinsbroek and Tijsseling [26] and Heinsbroek [27] obtained numerical solutions by coupling the fluid method of characteristics solution with two different beam theories for the piping—Bernoulli-Euler and Timoshenko. In addition, they solved the combined system using only the method of characteristics. It was concluded that the Bernoulli-Euler theory combined with a method of characteristics/finite element solution is sufficient for analyzing FSI in commercial piping systems.

Kojima and Shinada [28] performed tests on a thin-walled straight pipe that exhibited axial vibration due to Poisson coupling as well as vibration at the closed-free pipe end. A Lax-

Wendroff numerical method (see e.g., Mitchell and Griffiths [29]) was employed to predict the four variables of fluid velocity and pressure, and pipe velocity and strain, with comparisons shown between theory and experiment. Precursor waves were observed in their study. Poisson-coupled FSI in a long horizontal pipe excited by valve stroking was investigated by Elansary et al [30]. They compared the classic waterhammer solution with the FSI formulation and concluded that the latter gave improved results: Poisson coupling dampened the predicted pressure oscillations. They also concluded that frequency-dependent friction would also contribute to the damping. Vardy et al [31] isolated a suspended T-section in order to focus on the interactions between stress waves and pressure waves. They demonstrated that coupling at the boundaries might have a major influence on the resulting waveforms. As with many of the studies mentioned herein, they showed that FSI coupling alters the fundamental frequencies of oscillation when compared with those computed by isolating the liquid and structural components.

Frequency domain. Several investigators over the last decade have undertaken verification of frequency-based FSI models, most of which use analytical solutions rather than numerical ones. In their earlier-mentioned study Tenteralli [16], Brown and Tenteralli [17], and Tenteralli and Brown [18] obtained data from four experiments that were designed to isolate junction, Poisson, Bourdon, and frequency-dependent friction coupling (the latter restricted to the laminar flow regime). A hydraulic servo valve excited the fluid in the piping. In addition, he conducted experiments in a three-dimensional system that combined the junction mechanisms, Figures 11 and 12. System responses for frequencies up to 10000 Hz were recorded in some of the experiments. Data correlated well with Tenteralli's transmission matrix method of solution. Vibrations in a U-bend piping arrangement was investigated by Lesmez [15] and Lesmez et al [32] with frequencies up to 32 Hz supplied by an external mechanical vibrator. The data was used to verify an analytical model based on the matrix transfer method. Pressure measurements correlated better than displacement measurements, a result that has been observed in most reported studies. Jezequel et al [33] conducted a study that focused primarily on experimental data from a U-shaped pipe system. Their results were affected by the presence of cavitation and apparent nonlinear stiffness; consequently a high degree of damping was observed, although similarities were noted between calculated and measured displacement and pressure amplitudes and accompanying frequencies.

An experimental study performed by De Jong [20, 34] consisted of vibrating a liquid-filled pipe elbow at frequencies up to 500 Hz. Acceleration and pressure frequency spectra were used to verify a transfer-matrix analytical model derived from the Timoshenko beam equations and combined with the Poisson-coupled waterhammer relations. The model accurately predicted the spectra up to 250 Hz; beyond that frequency, differences were attributed to inaccurate representation of the flanged connections, the elbow, and lumped masses at the pipe ends. Svingen [21,22] published vibration data collected in an L-shaped pipe system, with excitation provided by a specially designed oscillating valve that had an operational range up to 1000 Hz, Figures 9 and 10. The data showed some discrepancy when compared with a finite-element frequency-domain model. Zhang et al [35] compared their Laplace transform model with improved data obtained in a repeat of the experiment published by Vardy and Fan [36]. A liquid-filled pipe freely supported in a horizontal plane was subjected to an axial impulsive force that induced junction coupling at each end of the pipe along with distributed Poisson coupling. Good agreement between measured and calculated natural frequencies was noted, especially among the lower fluid and structural modes. Jiao et al [37] presented experimental frequency spectra obtained in 1D, 2D and 3D oil-filled steel pipe systems. Their theoretical results included the effects of unsteady laminar friction.

5.2 Field measurements

Erath et al [38, 39] published two related studies that demonstrate FSI in a complex industrial piping system, Fig. 13. They provide data for a pipe system with pump shutdown and valve closing from the nuclear power plant KRB II (Gundremmingen, Germany). Six system fluid pressures, nine bending and torsion structural moments, and three structural displacements were numerically predicted and compared with recorded waveforms, Fig. 14. Their model consisted of utilizing two solutions in a predictor-corrector mode: a finite-difference waterhammer code coupled with a finite element structural solution. Even though no Poisson coupling was incorporated, the numerical predictions conform as well as can be expected to the measurements, especially for the first six fundamental periods of system oscillation. Uncoupled FSI calculations were also made, and it was shown that coupled FSI more accurately predicts the true system response. It was noted that in contrast to the conclusions reached by Heinsbroek and Kruisbrink [24], the predicted waveforms are more damped when coupled FSI analysis is employed as opposed to the uncoupled scenario.

Diesselhorst et al [9] included FSI and unsteady friction in a waterhammer code to obtain a more realistic damping behavior of pressure surges. Data measured during a pump trip in the feedwater system of a nuclear power station confirmed the effects of FSI and unsteady friction. FSI gave increased damping, reduced anchor forces, and changed resonance behavior.

5.3 Numerical and parametric studies

Time domain. The applied research group of engineers and scientists working at Delft Hydraulics Laboratory have conducted an extensive set of numerical experiments that served to enforce the concept of coupled FSI analysis, gain further refinement related to the methods of calculation, and better understand the various mechanisms that constitute the interaction process. Lavooij and Tijsseling [40] reported the use of two different numerical models for FSI: 1) solution of both the liquid and structural governing equations by the method of characteristics (MOC), and 2) solving the liquid equations by the method of characteristics and the structural equations by finite elements (MOC-FEM). The former utilized the Timoshenko beam theory, and the latter the Bernoulli-Euler beam theory. Both models include all of the basic coupling mechanisms. A provisional guideline was presented that suggests when interaction may be important:

$$T_{cef} < T_s < T_w \quad (5.1)$$

in which T_{cef} = effective system excitation time, T_s = eigen period of the structure, and T_w = fundamental period of waterhammer. If the structural mode is related to axial motion, then Poisson coupling may be significant. Heinsbroek et al [41] compared the MOC and MOC-FEM models to two test problems and concluded that for axial vibration the MOC model was preferable since it leads to exact solutions, but that for lateral vibration very fine computational grids were required when compared with the MOC-FEM procedure. Heinsbroek and Tijsseling [26] studied this theme further by applying the solutions to a straight pipe subjected to an impact load and to a single-elbow pipe excited by a rapid valve closure. The effects of rotary inertia and shear deformation were investigated using the two models. It was shown that the Bernoulli-Euler model failed when extreme impact loadings are present, but that for practical pipeline systems, it provides adequate predictions.

Heinsbroek [42] made a comparison between uncoupled and coupled FSI predictions. Using the Delft Hydraulics Laboratory large-scale three-dimensional test rig, he concluded that

uncoupled analysis failed to predict properly the dynamic Tresca stresses, and that the coupled model provided more accurate results. Heinsbroek and Tijsseling [43] studied the effect of support rigidity on the predicted waveforms from the Delft test rig. In particular, they focused on two items: the validity of uncoupled FSI, and magnitudes of extreme pressures and pipe stresses. The results showed that for the given test system, uncoupled FSI fails when the rigidity of the bend supports is less than the axial stiffness of one meter of pipe, and that maximum stresses seem to be higher in more flexible pipe systems, but the resulting forces on the supports are lower. They also presented an interesting diagram that shows how the main frequency of the pressure waveform varies with the assumed rigidity of the bend supports, Fig. 15. Erath et al [38] explained this behavior in terms of two idealized and coupled mass-spring systems, where one system represented the liquid and the other the solid. Additional parametric analyses were performed by Tijsseling and Heinsbroek [44] using the Delft rig data to determine the effect of bend motion. The contribution of each bend, as well as the effects of combinations of bends, on the predicted pressures and stresses was examined. The study clearly demonstrated how pipe and bend vibrations introduce the now well-established higher frequency components in the classical waterhammer waveform, with resulting pressures up to 100% higher than those predicted by the Joukowsky equation.

Tijsseling [45] revisited the simple four-equation model, with Poisson coupling being the only FSI mechanism. He demonstrated the presence of a beat in the predicted pressure waveform which he termed a Poisson-coupling beat; friction was not included in the formulation, so that damping of the signal did not occur. Bouabdallah and Massouh [46] also utilized the four-equation model to predict axial-mode FSI. In the study, time-line interpolations were employed for the fluid characteristics; the authors reported that accompanying damping effects were negligible for the conditions posed in their simulations. Gorman et al [47] revisited the axial-coupled model with an independent derivation that included the effects of radial shell vibration and initial axial tensional stress within the pipe. Using a finite-difference solution for the structural equations combined with the method of characteristics for the liquid, they compared their predictions of oscillatory flow with a simplified model developed by Lee et al [48]. Both models included lateral as well as axial motions, in contrast to the formerly discussed four-equation axial models; in that respect, they were more inclusive.

Frequency domain. Several groups have carried out investigations that relate to modeling in the frequency domain. A refined analytic transfer matrix model for axial fluid and pipe vibrations was reported by Charley and Caignaert [49], in which they included the variation of the pipe wall cross-section in addition to axial pipe force and velocity, and fluid pressure and velocity. Their model was compared with the more common model neglecting the area variation, and it showed a better match with measured data up to 2000 Hz. Zhang et al [7] applied the Laplace transform to the Poisson-coupled axial FSI equations that included quasi-steady laminar friction. The accuracy of their model compared favorably with experimental data and earlier developed formulations.

Svingen [21, 22, 50] described a finite element model for FSI in piping; the formulation includes axial vibration with Poisson coupling as well as bending, torsion, and junction coupling. The model was verified using laboratory data for a single elbow-vibrating pipe, and simulations were performed showing the effects of various types of coupling on pressure and displacement spectra. A similar study was performed by Gajić et al [51,52], wherein their model included linearized friction damping. Svingen's model was extended (Svingen and Kjeldsen [53], Svingen [54]) to include a novel Rayleigh-like damping term for the fluid motion. By analogy, the mass proportional damping was associated with linearized steady-state friction, and the stiffness proportional term with frequency-dependent friction. Svingen and Gajić compared their methodologies in a joint study [Svingen et al, 55]. Lastly, Moussou et al [56] analyzed Z-shaped piping that contained two vibrating elbows using both a 3-dimensional and a simplified 1-dimensional numerical code. They compared two piping/fluid models: one where the mass of the fluid is added to the mass of the pipe wall and the other a fully coupled FSI model. The correct latter approach leads to a description of the coupled modes of vibration (Fig. 16) and the development of a transfer function relating the structural displacement to the applied pressure perturbation.

6 INDUSTRIAL APPLICATIONS OF THE STANDARD FSI MODEL

Though yet in its infancy, interactive FSI analysis is beginning to find a niche in industrial applications. In this section we describe studies that relate to several significant issues related to fluid-piping motion: piping anchors and supports, noise, vibration, and seismic loads.

6.1 Anchor and support forces

A limited number of investigations have provided information related to the manner in which waterhammer forces are transmitted from piping to the pipe anchors and support mechanisms and vice versa. Two papers are quantitative while the remaining ones qualitatively deal with the subject matter. An early detailed study by Bürmann and Thielen [57] presented measured pressure, strain, and accelerations from a firewater pipeline subjected to transient excitation. They recognized the presence of precursor waves resulting from the Poisson coupling, and successfully modeled the axial waveforms using the extended method of characteristics. Later, Tijsseling and Vardy [58] investigated the effect of a pipe rack on the dynamic axial behavior of a single pipe element. Pressures and velocities were induced by axial impact of a pipe suspended on a rack by a steel rod. Coulomb friction was used to model the resistance between the pipe rack and the moving pipe. The measured forces were very small, yet reasonable agreement was found between measurement and coupled FSI analysis. A simple quantitative design guideline was proposed to assess the possible influence of axial support friction.

Raschke et al [59], Hamilton and Taylor [60] and Locher et al [61] present qualitative discussions about FSI in a variety of industrial piping systems. They provide evidence of support performance breakdown caused by a variety of excitations: condensation-induced waterhammer, priming of a liquid pipeline, pump trip on a ship-loading pipeline, and pump startup in a cooling water system that contained vapor pockets. Hamilton and Taylor [62] and Locher et al [61] respectively give guidelines regarding acceptability criteria and practical approaches and constraints to effective modeling of FSI. Lastly, Chary et al [63] reported observations in a boiler feed discharge-piping system in which a pipe vibrates off of its supports; they performed a transient FSI analysis using an uncoupled procedure.

6.2 Noise reduction

Vibrations in liquid-filled piping systems are sources of airborne (audible) noise; consequently

FSI analysis plays an important role in the understanding of noise generation and in dealing with means to mitigate such noise. The transfer matrix technique was employed by Kwong and Edge [64] to compare experimental data from two pipe configurations that were excited up to 5000 Hz. They showed that it was necessary to include laminar frequency-dependent friction in their analysis to obtain a better match with the experimental pressure and acceleration data. Subsequently, Kwong and Edge [65] incorporated their analytical method into an optimization procedure using genetic algorithms to determine the position of pipe clamps that minimize noise generation. Experimental results confirmed that significant noise reduction could be obtained by this technique.

De Jong and Janssens [66] describe a procedure to quantify the contribution of fluid-borne sound from machinery in piping. The equivalent-forces technique employs matrix inversion of measured transfer functions from excitation force to pipe response, with subsequent calculation of radiated sound pressure using so-called equivalent force and response positions. They note that it is necessary to properly account for seven (instead of six) degrees of freedom in a fluid-filled pipe. Janssens and Verheij [67], using laboratory data from a water-filled pipe system that represented the cooling-water pipe of a ship diesel engine, subsequently employed the methodology. Their predictions of sound pressure spectra trended with the measured spectra and they demonstrated the need for including the correct number of degrees of freedom.

6.3 Vibration damping

Experimental studies have been undertaken to reduce the vibrations that may occur due to liquid-pipe coupling. Tijsseling and Vardy [68] fitted a short section of ABS piping to a water-filled steel pipe, and excited axial vibration in the system with an impact rod. They successfully modeled the interactive waveforms using the extended method of characteristics algorithm. From both numerical predictions and experimental data, they concluded that the short plastic extension altered the vibration of the steel pipe by reducing the frequency of response, but not significantly reduced the amplitudes, and noted that a longer plastic section would result in lower amplitudes.

Munjal and Thawani [69] employed the model of Lesmez et al [32] to calculate the transfer and loss of power in a 500-mm long oil-filled composite-rubber hose; their application was focused on isolating vibrating machinery in the automotive industry. They concluded that Poisson coupling was not of much significance, and that transmission losses in Bernoulli-Euler beams were

found to be substantially lower than in Timoshenko beams. Additionally, pipe bends seemed to be beneficial for isolating vibration.

Koo and Park [70] describe a methodology to reduce vibrations in piping by spatially placing supports in a periodic fashion along a pipe axis. They describe that a pipe constrained in this manner possesses special characteristics known as wave stop and wave propagation frequency bands, or in other words, the system responds with apparent band-pass and band-reject filters. Employing predictive models using transfer-matrix methods combined with experimental data on two piping systems, they conclude that responses can be suppressed with periodically placed supports provided that the excitation frequencies are within wave stop bands.

6.4 Earthquake engineering

There have been several studies reported that deal with seismic loadings on liquid-filled piping. Hara [8] analyzed a liquid sodium-filled Z-shaped piping system subjected to a one-directional seismic excitation. The bending motion of the piping and the waterhammer were formulated in the frequency domain, and, using modal analysis, a two-degree-of-freedom set of equations was obtained for the fundamental vibration modes of the coupled system. Random, artificially generated, seismic loads were used to determine safety factors for a range of piping configurations. It was concluded that coupling effects were significant when the frequency ratio between the pressure wave and the pipe vibration ranged from 0.5 to 2, and the magnitude of the pressure wave induced by the coupling reached about 0.7 to 1.0 kPa per 1Gal of excitation. Hatfield and Wiggert [71] conducted a numerical study in which an aboveground three-dimensional pipe system was subjected to simulated earthquake ground motion; the motion was directed to excite the fundamental mode of the piping. The piping was filled with non-moving liquid, and component synthesis was used assuming no Poisson coupling. It was found that allowing the piping to be rigid produced an upper-bound estimate of pressure, and conversely, assuming the liquid to be incompressible resulted in underestimating displacement of the piping.

Bettinali et al [72] studied the effect of earthquake motion along the axial length of a single pipe. They described the development of a coupled FSI model that includes liquid column separation, but no Poisson coupling. A calculation of a postulated seismic load on the pipe showed that coupled analysis predicts lower pressure amplitudes than uncoupled analysis. Ogawa et al [73] applied an analytical model of earthquake-induced fluid transients to an in-place underground piping network. Using an artificially modified earthquake for excitation

combined with frequency-domain analysis, they concluded that induced sub-atmospheric pressures in the liquid were possible, and demonstrated how two parallel pipes in the same network could have one fail axially while the other experienced no damage, because of the different waterhammer response in each pipe.

7 EXTENSION OF THE STANDARD FSI MODEL

Studies have been undertaken to broaden the application of interactive FSI analysis. Refinements include incorporation of a non-elastic pipe material with possible failure, addition of centrifugal and Coriolis forces for slightly compressible flows in piping, distributed coupling mechanisms, the effect of pipe curvature, friction coupling, and cavitation. In addition several alternative numerical methods are discussed.

7.1 Non-elastic pipe wall material

A fair number of contributions include incorporation of visco-elastic and plastic wall properties into FSI analysis; this work was primarily motivated by concern related to pipe rupture in nuclear reactor piping systems (ignoring FSI work in hemodynamics, e.g. Rutten [74]).

Rachid and Stuckenbruck [75] combined a Kelvin-Voigt linear visco-elastic wall model with the extended axial method of characteristics that included Poisson coupling, assuming that the pipe and liquid wave speeds remained constant. In addition to obtaining comparisons with published data for a polyethylene straight pipe, they also modeled FSI in a two-elbow pipe system, and demonstrated the effects of relaxing constraints at the elbows.

Rachid et al [76] and Rachid and Costa Mattos [77] introduced a general constitutive theory of non-elastic wall behavior based on irreversible thermodynamics. The concept encompasses a number of rate-dependent theories of plasticity and allows description of viscous phenomena such as creep and relaxation. A modified method of characteristics that included Poisson coupling was used to model rapid valve closure in single-reach and articulated steel piping. A similar wall constitutive model was presented by Rachid et al [78] that included the possibility of elastic-plastic behavior in addition to elastic/visco-plastic behavior. In addition, operator splitting was combined with the method of characteristics to solve for the system variables. In contrast to the previous papers, Poisson coupling was not incorporated into the model.

Rachid et al [79, 80] recognized the need to incorporate a variable liquid wave speed, one that can reduce its magnitude significantly when a pipe material is approaching a plastic state. To account for this phenomenon, they solved the nonlinear wave equations using Glimm's method combined with operator splitting. In Rachid et al [79] elastic-plastic wall behavior was considered, and numerical examples were presented that illustrated the evolution of damage

induced by pressure pulses traveling in a straight stainless steel pipe. By contrast, Rachid et al [80] included plastic behavior and modeled pipe failure in a straight stainless steel pipe induced by instantaneous valve closure. Neither of the two studies included Poisson coupling. That omission was corrected in Rachid et al [81], where the modeling scenario described in Rachid et al [79] was revisited. The effect of axial-induced pipe motion was shown to significantly alter the predicted pipe damage. Recognizing that the wave speed reduces as the pipe wall approaches a plastic state, Rachid and Costa Mattos [82] performed a parametric study on the effect of employing the low Mach number assumption in their solution techniques. They concluded that the assumption was valid for metallic tubes, but for plastic tubes, its validity is dependent upon the manner in which the pipe fails.

Yu and Kojima [83] developed an analytic model employing the transfer matrix method that described FSI in a liquid-filled anisotropic visco-elastic pipe. They experimentally determined the mechanical properties of the pipe material assuming a Kelvin-Voigt wall model, and collected transfer matrix parameter data in a flexible hydraulic hose. Their analytic model compared well with the experimental results over a frequency range of 0-3 kHz. In addition to their developed model, the data was compared with the visco-elastic model developed by Suo and Wylie [84] in which the axial motion of the pipe was neglected; it was shown that Suo and Wylie's model approximated the experimental data below frequencies of 1 kHz.

7.2 Centrifugal and Coriolis forces

It is evident that a laterally vibrating pipe accelerates its contained fluid. This is properly taken into account through the inertia term, $\rho_f A_f \partial^2 u_y / \partial t^2$, in Eq. 2.13. Less evident is the fact that a laterally vibrating pipe is (slightly) curving and rotating everywhere, so that centrifugal (V_0^2 / R_c) and Coriolis ($2 V_0 \dot{\theta}_x$) accelerations in the fluid (having flow velocity V_0) generate lateral forces. Including these forces in a Bernoulli-Euler beam model yields the standard equation

$$(\rho_t A_t + \rho_f A_f) \frac{\partial^2 u_y}{\partial t^2} + E I_t \frac{\partial^4 u_y}{\partial z^4} + \rho_f A_f V_0^2 \frac{\partial^2 u_y}{\partial z^2} + 2 \rho_f A_f V_0 \frac{\partial^2 u_y}{\partial t \partial z} =$$

(7.1)

where V_0 is the steady state flow velocity relative to the pipe. The third term is the centrifugal

force, thereby noting that $\partial^2 u_y / \partial z^2$ approximates the local pipe curvature ($1/R_c$). This centrifugal term is a factor A_f / A_{nozzle} larger for a pipe terminated by a convergent nozzle. The last term is the Coriolis force, noting that $\partial^2 u_y / \partial t \partial z$ is the local rotational pipe velocity.

Païdoussis [85] gives an encyclopedic treatise of the subject, with focus on stability analysis and dynamics. In his Section 3.2 it is shown that as a result of the flow-induced centrifugal force, a pipe supported at its ends will buckle at the critical flow velocity $\pi (E I_t / \rho_f A_f)^{1/2} / L$. A cantilevered pipe will, at sufficiently high flow velocity, lose stability by flutter. However, for industrial systems stability problems are not to be expected. Citing Païdoussis [85, p. 267]: "the effect of internal flow on the dynamics of pipes conveying fluids begins to become interesting, let alone worrisome, at flow velocities at least ten times those found in typical engineering systems." Centrifugal and Coriolis forces are of importance in systems experiencing very high flow velocities and in systems of high flexibility, in which case large-deflection analysis is needed.

Païdoussis [85] concentrates on the dynamic behavior of the *pipe*. The *flow* is considered as uniform and steady (or unsteady in the sense of small harmonic perturbations, thereby taking into account fluid inertia but neglecting fluid elasticity). Dynamics of the fluid and back coupling from the lateral pipe vibration are ignored. Axial pipe motion is neglected, except in the large-deflection analysis of a pipe with fixed ends (in which case Poisson coupling was omitted). Research taking into account fluid dynamics and axial pipe vibrations, thus linking Païdoussis-type models to the waterhammer-FSI model of Section 2, is considered in this section. This linking of models can be of significance in multi-pipe systems where lateral and axial (pipe and fluid) vibrations interact at unrestrained elbows and branches (junction coupling).

Apparently the first attempt to link the aforementioned models was by Zhuge *et al.* [86]. The observed damping in an experimental FSI test rig was predicted by complex modal analysis, but it was not made clear whether the computed damping came from frequency-dependent friction or from Coriolis forces. Stittgen and Zielke [87] studied the dynamic behavior of flexible curved tubes subjected to external and internal (waterhammer) loads. Centrifugal and translatory accelerations found from large tube motions were fed into waterhammer equations in which the flow velocity was taken relative to the pipe. The (because of large deflections) structural motion was calculated with the FEM, the fluid dynamics with the MOC, and an iterative solution coupled the motion. The method was applied to an offshore riser and a harbor loading line.

Piet-Lahanier and Ohayon [88] used decoupled equations for lateral and axial pipe motion. The lateral equations were similar to Eq. 7.1 and the axial equations were linearized around the steady state. In the waterhammer-type equations for the fluid, the mass flow rate was taken relative to the pipe. Poisson coupling was not taken into account and assemblies of straight pipes represented curved pipes. The governing equations were solved in the frequency domain by the FEM. Piet-Lahanier and Ohayon compared their numerical solutions for a simply-supported flexurally-vibrating pipe with experimental data by Dodds and Runyan [89]. A 2.8-m-long aluminum alloy pipe of 162-mm inner diameter and 3-mm wall thickness carried water at increasing flow rates. Table 1 gives theoretical (for $V_0 = 0$) and computed natural frequencies. It is seen that the pipe's natural frequencies hardly change if the flow velocity is below 10 m/s. For higher velocities, it is interesting to see that the first natural frequency decreases with increasing velocity, until it finally vanishes at the critical velocity (153 m/s theoretically). At this point the pipe has lost its stiffness and will buckle. This behavior is confirmed in Figure 17, noting that the experimental data shown were argued by Païdoussis [85, p. 105].

For coupled lateral-axial motion in a one-elbow pipe system, Piet-Lahanier and Ohayon [88] verified computed solutions against experimental results by Davidson and Smith [90], and against numerical results by Everstine [91]. It must be noted that the experimental data of Davidson and Smith, having been used by many others for validation purposes, were questioned by Brown and Tentarelli [92, p. 148] concerning the flexibility of an assumed rigid support. Computations with a 50-m/s flow in the one-elbow system led to a much-increased damping at frequencies below the second natural frequency. The small influence of FSI on the one-elbow system's natural frequencies was tabulated.

Lee et al [48, 93] combined the dynamic equations of Païdoussis and Issid [94] describing lateral pipe vibration with the dynamic equations for axial vibration (pipe and fluid) of Wiggert et al [6], thereby neglecting Poisson coupling. Compared with Equation 7.1, the lateral equations allowed for flow unsteadiness. The latter was introduced through small-amplitude sinusoidal oscillations on top of a steady flow, thereby neglecting fluid elasticity so that uniform flow conditions prevailed. A stability analysis was performed for a simply supported straight pipe. Improved equations, including Poisson coupling, were presented by Lee and Kim [95] and solved in the time domain by the FEM. The equations were further complicated by Gorman et al [47] to account for large deflections and radial shell deformations.

Wang and Tan [96] used Eq. 7.1 in a quasi-steady fashion (V_0 simply replaced by V) for a

fully coupled FSI analysis in line with the theory in Section 2. Solutions were obtained from an iterative FSI procedure combining MOC (fluid) and FEM (structure). Figure 18 shows the small effect of centrifugal and Coriolis forces on the dynamic pressure in a steel single-elbow reservoir-pipe-valve system where water initially flowing at a velocity of 15 m/s was suddenly stopped. The method was applied to an aircraft hydraulic system in [Wang and Tan, 97].

7.3 Distributed axial-lateral coupling

The influence of axial flow on lateral vibration is discussed in Section 7.2; other (no-flow) axial-lateral couplings are addressed here.

It is well known that large axial forces affect the *lateral* vibration of straight beams (e.g. Clough and Penzien [98, p. 296], Weaver et al [99, p. 454]). It is also known that large internal pressures *may* stiffen fluid-filled pipes (e.g. Païdoussis [85, p. 98]). These effects have not been included in the model described in Section 2.1. How lateral displacements and forces influence *axial* vibrations is less clear. Vardy and Alsarraj [100] investigated axial-lateral coupling in beams, thereby taking into account an axial momentum flux due to rotational velocities caused by bending. Païdoussis [85, p. 287] presented equations for the large-deflection behavior of a pipe fixed at both ends, which possess many coupling terms. Gorman et al [47] extended Païdoussis's equations with unsteady flow terms and equations. Budny [10] and Fan [101] observed pressure variations generated by the lateral vibration of a straight liquid-filled pipe. These might be explained by the axial-lateral coupling mechanisms mentioned above, in combination with Poisson and Bourdon coupling. Axial-lateral coupling is evident in the (initially) curved pipes considered in Section 7.4.

It is noted that axial-lateral coupling occurs at most types of practical pipe supports; these local effects may dominate the distributed effects mentioned above.

7.4 Curved pipes

The mathematical model presented in Section 2.1 is valid for straight pipes connected by relatively short bends (and junctions). For curved pipes and bends that are long compared to the adjacent straight pipes more advanced modeling is needed. Valentin et al [102] and Hsu and Phillips [103] developed theory for fluid-filled tubes of constant curvature. The strong coupling of axial and lateral waves in the in-plane motion of a curved pipe was described by eight first-order equations. The beam-type model included Poisson coupling and it is a natural extension of the basic equations shown in Section 2.1. If R_c denotes the radius of curvature, the following terms (with the correct signs) have to be added to the first-order equations in Section 2.1: $(1 - 2\nu) \dot{u}_y / R_c$ to Eq. 5.3,

$Q_y / (e_t A_t R_c)$ to Eq. 5.6, \dot{u}_y / R_c to Eq. 5.7, $(A_f P - A_t \sigma_z) / R_c$ to Eq. 5.9 and \dot{u}_z / R_c to Eq. 5.10. Note that $R_c = \infty$ gives the original straight-pipe equations. For curved pipes with high-velocity steady flow and neglecting dynamic Poisson effects, Chen [104, 105] derived governing equations with terms for centrifugal and Coriolis forces; see also (Païdoussis [85, p. 424-425]). In addition, Dupuis and Rousselet [106] provide first-order large-deformation (small-strain) equations with in-plane/out-of-plane coupling terms.

Valentin et al [102] performed an interesting parameter variation study in the frequency domain from which they concluded that for relatively thick-walled pipes low-frequency pressure waves are about 15% reflected (85% transmitted) at unrestrained bends, virtually independent of frequency, radius of curvature and bend angle (between 90 and 180 degrees). High-frequency pressure oscillations are not reflected at bends. Hsu and Phillips [103] solved the eight coupled equations in the time domain with the MOC to study the effect of bend motion on a propagating pressure pulse. The predicted 90% transmission was confirmed by experiment. Tentarelli [16], Brown and Tentarelli [17], and Tenteralli and Brown [18] extended the model of Valentin et al [102] with Bourdon coupling, which includes reduced flexibility due to ovalization. De Jong [20] adopted Valentin et al's model, but introduced a flexibility factor $k_p = 1.65 R^2 / (e R_c)$ by using EI_r / k_p instead of EI_r in Eq. 5.12, to account for ovalization effects. It is noted that flexibility factors also depend on the fluid pressure, as shown in Figure 19. A handy formula for k_p is [Dodge and Moore, 107]:

$$k_p = \frac{1.66 \lambda^{-1}}{1 + 1.75 \lambda^{-4/3} e^{-1.15 \psi^{-1/4}}} \quad \text{for } 0.05 \leq \lambda \leq 1.0 \text{ and } 0 \leq \psi \leq 0.1 \quad (7.2)$$

where

$$\lambda = \frac{e R_c}{R^2 \sqrt{1 - \nu^2}} \quad \text{and} \quad \psi = \frac{P R_c^2}{E R e}$$

are dimensionless parameters characterising the bend and the internal pressure, respectively.

Modeling curved pipes through appropriate PDE is theoretically elegant, but the simple and practical approach of using a series of short straight sections (with reduced flexibility due to ovalization) connected by miter bends (see Figure 20 and Eqs. 5.18) gives amazingly good results. De Jong [20] showed—for the bend in Figure 21—that both methods give the same result, Fig. 21a. Table 2 lists the comparison with FEM results in which the bend was simulated by 1008 eight-node shell elements with 12 elements on the pipe circumference.

7.5 Damping and friction

The standard FSI model of section 2.1 is energy conserving, as damping and friction mechanisms have not been taken into account. Damping occurs in materials because relaxation processes result in stresses and strains that are out of phase. Friction is a consequence of interfacial shear. For industrial systems, it may roughly be stated that structural free vibrations dampen because of rubbing at supports and fluid transients dampen because of wall friction. Structural damping is commonly modelled in a practical way by one parameter accounting for all dissipative mechanisms. In a frequency-domain analysis taking a complex-valued modulus of elasticity conveniently accounts for this. In FEM procedures, a Rayleigh damping matrix can be applied in both time and frequency domains. Fluid damping along pipes comes from wall friction. Quasi-steady models, where the friction force depends on fluid velocity, and unsteady models, where it also depends on temporal fluid accelerations, are mostly used. For FSI analyses the fluid velocities must be applied relative to the axial wall motion. The effect of non-zero radial pipe wall velocities has always been neglected. Rayleigh damping to account for fluid friction was proposed by Svingen [54], see Section 5.3.

Leslie and Tijsseling [108] reviewed the manner in which FSI researchers included friction and damping in their models. They found that studies by Budny et al [109, 110] and by Tijsseling and Vardy [58] focused on damping effects. Budny et al [110] investigated the influence of structural damping on pressure oscillations in a single pipe. For a virtually unrestrained pipe, they found that ignoring structural (viscous) damping in their FSI four-equation model would give pressures that are 20-25 percent higher than measured values. Tijsseling and Vardy [58] investigated, theoretically and experimentally, the influence of dry friction on fluid pressures for a single pipe sliding on one support.

Leslie and Tijsseling [111] studied wave speeds describing propagating disturbances under transient conditions and phase velocities describing wave trains under steady-oscillatory conditions for axial, lateral and torsional vibration of liquid-filled pipes. Distinguishing between ideal, dispersive and dissipative systems, they demonstrated the influences of fluid friction, viscous structural damping, and FSI on the various wave speeds and phase velocities.

It is noted that some engineers propose, as a gross simplification, to model FSI itself as increased damping (e.g., Kruisbrink [112], Erath et al [38, 39]).

7.6 Cavitation

The impact loads produced by collapsing voids at dead ends are adequately described by Eqs. 2.20.

Similar relations can be used for voids formed at any other location in the system. In fact, regions of distributed cavitation (two-phase flow) can reasonably well be represented by a series of small lumped voids (e.g. Wylie [113], Zielke and Perko [114]). Fan and Tijsseling [115] and Tijsseling et al [116] have made a study of the simultaneous occurrence of cavitation and FSI. In Fan and Tijsseling [115], numerical simulation and experiment concerned a single pipe; in Tijsseling et al [116], a second pipe was added to form a one-elbow system. Other work combining FSI and cavitation has been summarised by Tijsseling [1].

7.7 Alternative numerical methods

Section 2.2 describes how the method of characteristics (MOC) and the finite element method (FEM) are employed to solve the basic equations. Works that employ alternative numerical methods are mentioned here.

Hatfield and Wiggert [117] described a component synthesis procedure that is formulated in two phases. The first is a standard modal analysis of the piping and supports, and the second is a waterhammer analysis modified to account for the piping motion. The latter step combines a MOC formulation for the liquid and a modal description of the piping system coupled by force and flow equilibrium constraints at junctions. Finite-difference methods have been used by Mansour [118, 119] and Gorman et al [47]. Mansour applied an adapted Preissmann scheme (see e.g., Abbott and Basco [120]) to the FSI four-equation model. His method is implicit, non-iterative and not suitable for impact loads. Gorman et al used an explicit scheme to solve for axial, radial and lateral pipe motion, and, in a combination with MOC, for unsteady fluid flow. An iterative procedure accounted for FSI. The method was tested for a pipe subjected to steady flow with a harmonic pulsation. Greenshields et al [121] utilized the finite volume method to solve three-dimensional equations for both fluids and solids. Iterative coupling was obtained through moving fluid-structure interfaces. The method was capable to predict in detail the start of a propagating pressure wave (waterhammer) accounting for two-dimensional and pipe-response effects.

Bahrar et al [122] gave an even more detailed description of the initial evolution of a pressure wave. In a rigorous mathematical treatment they coupled two-dimensional equations for the fluid to shell equations for the pipe wall. Laplace-Carson transforms, their numerical inverses and asymptotic approximations yielded solutions in frequency and time domains. The complex solutions were successfully verified against direct numerical simulations. The influence of laminar viscosity was investigated. It was shown that an applied step pressure nicely evolved to a waterhammer wave accompanied by a precursor due to Poisson coupling, Fig. 22.

8 CONCLUSION

The understanding of fluid-structure interaction in piping systems—primarily those that exhibit waterhammer-like forces acting on piping and vice versa—has benefited by many investigations over the last several decades. In this review, we have attempted to capture the spirit and essence of those investigations, primarily from the last ten to fifteen years. It is gratifying to see that interest in the topic is increasing in both the research and industrial arenas.

More effort certainly needs to occur to bridge the gap between research and practice. That need has been succinctly stated in Locher et al [61]: “Fluid-structure interaction is a very complex problem that is highly dependent on the pipe layout. Generalization is not presently possible, and the calculations have to be treated on a case-by-case basis. At present, calculations involving forces with fluid-structure interactions are justified only for very critical systems such as nuclear power plants. It cannot be justified for industrial systems because: 1) there are too many supports to analyze all of them individually, and 2) with the present state-of-the-art, analyzing every support is not economical in today’s competitive environment. Future codes for fluid-structure interaction will have to be more user-friendly and much more economical to be used in the analysis of industrial process systems.”

We hope that this review will be of use to both researchers and practitioners, and that efforts will continue to bring the many useful contributions described herein to the point where meaningful, efficient, and practical industrial applications of FSI in piping systems will become commonplace.

REFERENCES

1. Tijsseling AS (1996), "Fluid-structure interaction in liquid-filled pipe systems: a review," *Journal of Fluids and Structures* **10** 109-146.
2. Wiggert DC (1986), "Coupled transient flow and structural motion in liquid-filled piping systems: a survey," *Proceedings of the ASME Pressure Vessels and Piping Conference*, Chicago, USA, Paper 86-PVP-4.
3. Wiggert DC (1996), "Fluid transients in flexible piping systems: a perspective on recent developments," *Proceedings of the 18th IAHR Symposium on Hydraulic Machinery and Cavitation*, Valencia, Spain, 58-67.
4. Cowper GR (1966), "The shear coefficient in Timoshenko's beam theory," *Journal of Applied Mechanics* **33** 335-340.
5. Hilber HM, Hughes TJR, and Taylor RL (1977), "Improved numerical dissipation for time integration algorithms in structural dynamics," *Earthquake Engineering and Structural Dynamics* **5** 283-292.
6. Wiggert DC, Otwell RS, and Hatfield FJ (1985), "The effect of elbow restraint on pressure transients," *Journal of Fluids Engineering* **107** 402-406. (Discussed by RE Schwirian and JS Walker in **108** 121-122.)
7. Zhang L, Tijsseling AS, and Vardy AE (1995), "Frequency response analysis in internal flows," *Journal of Hydrodynamics*, China Ocean Press, Beijing, Series B, **3**(3) 39-49.
8. Hara F (1988), "Seismic vibration analysis of fluid-structure interaction in LMFBR piping systems," *Journal of Pressure Vessel Technology* **110** 177-181.
9. Diesselhorst T, Schmidt R, and Schnellhammer W (2000), "Realistic calculation of pressure surges. Inclusion of dynamic friction and fluid/structure interaction," *3R international* **39** 678-682 (in German).
10. Budny DD (1988), "The influence of structural damping on the internal fluid pressure during a fluid transient pipe flow," Ph.D. Thesis, Michigan State University, Department of Civil and Environmental Engineering, East Lansing, USA.
11. Kruisbrink ACH and Heinsbroek AGTJ (1992), "Fluid-structure interaction in non-rigid pipeline systems—large scale validation tests," *Proceedings of the International Conference on Pipeline Systems*, BHR Group, Manchester, UK, 151-164.
12. Kruisbrink ACH and Heinsbroek AGTJ (1992), "Fluid-structure interaction in non-rigid pipeline systems—large scale validation tests," *Proceedings of the Second National Mechanics Congress*, Kerkrade, The Netherlands, ISBN 0-7923-2442-0, 57-64.
13. Enkel P and Grams J (1997), "Pressure surge analysis with regard to fluid structure interaction," *3R international* **36** 446-451 (in German).
14. Tijsseling AS and Fan D (1992), "Fluid-structure interaction and column separation in a closed pipe," *Proceedings of the Second National Mechanics Congress*, Kerkrade, The Netherlands, ISBN 0-7923-2442-0, 205-212.
15. Lesmez MW (1989), "Modal analysis of vibrations in liquid-filled piping systems," Ph.D. Thesis, Michigan State University, Department of Civil and Environmental Engineering, East Lansing, USA.
16. Tenteralli SC (1990), "Propagation of noise and vibration in complex hydraulic tubing systems," Ph.D. Thesis, Lehigh University, Department of Mechanical Engineering, Bethlehem, USA.
17. Brown FT and Tentarelli SC (2001), "Dynamic behavior of complex fluid-filled tubing systems—Part 1: Tubing analysis," *Journal of Dynamic Systems, Measurement, and Control*, **123** 71-77.

18. Tentarelli SC and Brown FT (2001), "Dynamic behavior of complex fluid-filled tubing systems—Part 2: System analysis," *Journal of Dynamic Systems and Control* **123** 78-84.
19. Frikha S (1992), "Analyse expérimentale des sollicitations dynamiques appliquées à une portion de structure en service modélisable par la théorie des poutres," Ph.D. Thesis, Ecole Nationale Supérieure des Arts et Métiers (ENSAM), Laboratoire de Mécanique des Structures, Paris, France (in French).
20. De Jong CAF (1994, 2000), "Analysis of pulsations and vibrations in fluid-filled pipe systems," Ph.D. Thesis, Eindhoven University of Technology, Department of Mechanical Engineering, Eindhoven, The Netherlands (Errata: April 2000).
21. Svingen B (1996), "Fluid structure interaction in piping systems," Ph.D. Thesis, The Norwegian University of Science and Technology, Faculty of Mechanical Engineering, Trondheim, Norway.
22. Svingen B (1996), "Fluid structure interaction in slender pipes," *Proceedings of the 7th International Conference on Pressure Surges and Fluid Transients in Pipelines and Open Channels*, BHR Group, Harrogate, UK, 385-396.
23. Wiggert DC, Hatfield FJ, and Stuckenbruck S (1987), "Analysis of liquid and structural transients by the method of characteristics," *Journal of Fluids Engineering* **109** 161-165.
24. Heinsbroek AGTJ and Kruisbrink ACH (1993), "Fluid-structure interaction in non-rigid pipeline systems—large scale validation experiments," *Transactions of SMiRT12*, Stuttgart, Germany, Paper J08/1.
25. Heinsbroek AGTJ and Kruisbrink ACH (1991), "*FLUSTRIN Phase 3 Validation Experiments and Simulations*," Research Report **J 526**, Delft Hydraulics, Delft, The Netherlands.
26. Heinsbroek AGTJ and Tijsseling AS (1993), "Fluid-structure interaction in non-rigid pipeline systems—a numerical investigation II," *Transactions of SMiRT12*, Stuttgart, Germany, Paper J08/2.
27. Heinsbroek AGTJ (1997), "Fluid-structure interaction in non-rigid pipeline systems," *Nuclear Engineering and Design* **172** 123-135.
28. Kojima E and Shinada M (1988), Dynamic behavior of a finite length straight pipe subject to water-hammer (2nd report, for a very thin-walled pipe). *Transactions of the Japan Society of Mechanical Engineers, Series B*, **54** 3346-3353 (in Japanese).
29. Mitchell AR and Griffiths DF (1980), *The Finite Difference Method in Partial Differential Equations*, John Wiley and Sons.
30. Elansary AS, Silva W, and Chaudhry MH (1994), "Numerical and experimental investigation of transient pipe flow," *Journal of Hydraulic Research* **32** 689-706.
31. Vardy AE, Fan D, and Tijsseling AS (1996), "Fluid/structure interaction in a T-piece pipe," *Journal of Fluids and Structures* **10** 763-786.
32. Lesmez MW, Wiggert DC, and Hatfield FJ (1990), "Modal analysis of vibrations in liquid-filled piping-systems," *Journal of Fluids Engineering* **112** 311-318.
33. Jezequel L, Khamlichi A, and Tephany F (1994), "Interpretation of fluid-structure interaction experiment in a frame pipe," *Sloshing, Fluid-Structure Interaction and Structural Response due to Shock and Impact Loads*, ASME -PVP **272** 1-12.
34. De Jong, CAF (1995), "Analysis of pulsations and vibrations in fluid-filled pipe systems," *Proceedings of the 1995 Design Engineering Technical Conferences*, Boston, USA, ASME-DE **84-2**, Vol. 3, Part B, 829-834.
35. Zhang L, Tijsseling AS, and Vardy AE (1999), "FSI analysis of liquid-filled pipes," *Journal of Sound and Vibration* **224**(1) 69-99.
36. Vardy AE and Fan D (1989), "Flexural waves in a closed tube," *Proceedings of the 6th International Conference on Pressure Surges*, BHRA, Cambridge, UK, 43-57.

37. Jiao Z, Hua Q, and Yu K (1999), "Frequency domain analysis of vibrations in liquid-filled piping systems," *Acta Aeronautica et Astronautica Sinica* **20**(4) 1-18 (in Chinese).
38. Erath W, Nowotny B, and Maetz J (1998), "Simultaneous coupling of the calculation of pressure waves and pipe oscillations," *3R international* **37** 501-508 (in German).
39. Erath W, Nowotny B, and Maetz J (1999), "Modelling the fluid structure interaction produced by a waterhammer during shutdown of high-pressure pumps," *Nuclear Engineering and Design* **193** 283-296.
40. Lavooij CSW and Tijsseling AS (1991), "Fluid-structure interaction in liquid-filled piping systems," *Journal of Fluids and Structures* **5** 573-595.
41. Heinsbroek AGTJ, Lavooij CSW, and Tijsseling AS (1991), "Fluid-structure interaction in non-rigid piping—a numerical investigation," *Transactions of SMiRT 11*, Tokyo, Japan, Paper B12/1, 309-314.
42. Heinsbroek AGTJ (1993), "Fluid-structure interaction in non-rigid pipeline systems—comparative analyses," *ASME/TWI 12th International Conference on Offshore Mechanics and Arctic Engineering*, Glasgow, UK, Paper OMAE-93-1018, 405-410.
43. Heinsbroek AGTJ and Tijsseling AS (1994), "The influence of support rigidity on waterhammer pressures and pipe stresses," *Proceedings of the Second International Conference on Water Pipeline Systems*, BHR Group, Edinburgh, UK, 17-30.
44. Tijsseling AS and Heinsbroek AGTJ (1999), "The influence of bend motion on waterhammer pressures and pipe stresses," *Proceedings of the 3rd ASME & JSME Joint Fluids Engineering Conference, Symposium S-290 Waterhammer* (Editor JCP Liou), San Francisco, USA, ASME-FED **248** 1-7.
45. Tijsseling AS (1997), "Poisson-coupling beat in extended waterhammer theory," *Proceedings of the 4th International Symposium on Fluid-Structure Interactions, Aeroelasticity, Flow-Induced Vibration and Noise*, Dallas, USA, ASME-AD **53-2** 529-532.
46. Bouabdallah S and Massouh F (1997), "Fluid-structure interaction in hydraulic networks," *Proceedings of the 4th International Symposium on Fluid-Structure Interactions, Aeroelasticity, Flow-Induced Vibration and Noise*, Dallas, USA, ASME-AD **53-2** 543-548.
47. Gorman DG, Reese JM, and Zhang YL (2000), "Vibration of a flexible pipe conveying viscous pulsating fluid flow," *Journal of Sound and Vibration* **230**(2) 379-392.
48. Lee U, Pak CH, and Hong SC (1995), "The dynamics of a piping system with internal unsteady-flow," *Journal of Sound and Vibration* **180**(2) 297-311.
49. Charley J and Caignaert G (1993), "Vibroacoustical analysis of flow in pipes by transfer matrix with fluid-structure interaction," *Proceedings of the 6th International Meeting of the IAHR Work Group on the Behavior of Hydraulic Machinery under Steady Oscillatory Conditions*, Lausanne, Switzerland, 1-9.
50. Svingen B (1994), "A frequency domain solution of the coupled hydromechanical vibrations in piping systems by the finite element method," *Proceedings of the 17th IAHR Symposium on Hydraulic Machinery and Cavitation*, Beijing, PR China, 1259-1269.
51. Gajić A, Pejović S, Stojanović Z, and Kratića J (1995), "Fluid-structure interaction analysis in frequency domain," *Proceedings of the 7th International Meeting of the IAHR Work Group on the Behavior of Hydraulic Machinery under Steady Oscillatory Conditions*, Ljubljana, Slovenia, Paper F5.
52. Gajić A, Pejović S, and Stojanović Z (1996), "Hydraulic oscillation analysis using the fluid-structure interaction model," *Proceedings of the 18th IAHR Symposium on Hydraulic Machinery and Cavitation*, Valencia, Spain, 845-854.
53. Svingen B and Kjeldsen M (1995), "Fluid structure interaction in piping systems," *Proceedings of the International Conference on Finite Elements in Fluids - New Trends and*

Applications, Venice, Italy, 955-963.

54. Svingen B (1997), "Rayleigh damping as an approximate model for transient hydraulic pipe friction," *Proceedings of the 8th International Meeting of the IAHR Work Group on the Behavior of Hydraulic Machinery under Steady Oscillatory Conditions*, Chatou, France, Paper F2.
55. Svingen B, Stojanović Z, Brekke H, and Gajić A (1997), "Two numerical methods of hydraulic oscillations analysis in piping systems including fluid-structure interaction," *Proceedings of the International Conference on Fluid Engineering*, JSME Centennial Grand Congress, Tokyo, Japan, 1601-1606.
56. Moussou P, Vaugrante P, Guivarch M, and Seligmann D (2000), "Coupling effects in a two elbows piping system," *Proceedings of the 7th International Conference on Flow Induced Vibrations*, Lucerne, Switzerland, 579-586.
57. Bürmann W and Thielen H (1988), "Measurement and computation of dynamic reactive forces on pipes containing flow," *3R international* 27 434-440 (in German).
58. Tijsseling AS and Vardy AE (1996), "Axial modelling and testing of a pipe rack," *Proceedings of the 7th International Conference on Pressure Surges and Fluid Transients in Pipelines and Open Channels*, BHR Group, Harrogate, UK, 363-383.
59. Raschke E, Seelinger P, Sperber A, and Strassburger R (1994), "Simulation des instationären Verhaltens verfahrenstechnischer Anlagen mit langen Rohrleitungen," *Chem.-Ing.-Tech* 66 652-660 (in German).
60. Hamilton M and Taylor G (1996), "Pressure surge – Case studies," *Proceedings of the 7th International Conference on Pressure Surges and Fluid Transients in Pipelines and Open Channels*, BHR Group, Harrogate, UK, 15-27.
61. Locher FA, Huntamer JB, and O'Sullivan JD (2000), "Caution—pressure surges in process and industrial systems may be fatal," *Proceedings of the 8th International Conference on Pressure Surges*, BHR Group, The Hague, The Netherlands, 3-18.
62. Hamilton M and Taylor G (1996), "Pressure surge – Criteria for acceptability," *Proceedings of the 7th International Conference on Pressure Surges and Fluid Transients in Pipelines and Open Channels*, BHR Group, Harrogate, UK, 343-362.
63. Chary SR, Kumar GV, Rajamani A, and Rao CVK (1998), "Transient response of a boiler feed pump discharge pipeline—a case study," *Proceedings of the 16th International Modal Analysis Conference*, Santa Barbara, USA, 1-10.
64. Kwong AHM and Edge KA (1996), "Structure-borne noise prediction in liquid-conveying pipe systems," *Proceedings of the Institution of Mechanical Engineers Part I - Journal of Systems and Control Engineering* 210(3) 189-200.
65. Kwong AHM and Edge KAA (1998), "A method to reduce noise in hydraulic systems by optimizing pipe clamp locations," *Proceedings of the Institution of Mechanical Engineers Part I - Journal of Systems and Control Engineering* 212(I4) 267-280.
66. De Jong CAF and Janssens MHA (1996), "Numerical studies of inverse methods for quantification of sound transmission along fluid-filled pipes," *Proceedings of Internoise 96*, Liverpool, UK, 3203-3206.
67. Janssens MHA and Verheij JW (1999), "The use of an equivalent forces method for the experimental quantification of structural sound transmission in ships," *Journal of Sound and Vibration* 226(2) 305-328.
68. Tijsseling AS and Vardy AE (1996), "On the suppression of coupled liquid/pipe vibrations," *Proceedings of the 18th IAHR Symposium on Hydraulic Machinery and Cavitation*, Valencia, Spain, 945-954.
69. Munjal ML and Thawani PT (1997), "Prediction of the vibro-acoustic transmission loss of

- planar hose-pipe systems,” *Journal of the Acoustical Society of America* **101** 2524-2535.
70. Koo GH and Park YS (1998), “Vibration reduction by using periodic supports in a piping system,” *Journal of Sound and Vibration* **210**(1) 53-68.
 71. Hatfield FJ and Wiggert DC (1990), “Seismic pressure surges in liquid-filled pipelines,” *Journal of Pressure Vessel Technology* **112** 279-283.
 72. Bettinali F, Molinaro P, Ciccotelli M, and Micelotta A (1991), “Transient analysis in piping networks including fluid-structure interaction and cavitation effects,” *Transactions SMiRT 11*, Tokyo, Paper K35/5, 565-570.
 73. Ogawa N, Mikoshiha T, and Minowa C (1994), “Hydraulic effects on a large piping system during strong earthquakes,” *Journal of Pressure Vessel Technology* **116** 161-168.
 74. Rutten MCM (1998), “Fluid-solid interaction in large arteries,” Ph.D. Thesis, Eindhoven University of Technology, Department of Mechanical Engineering, Eindhoven, The Netherlands.
 75. Rachid FBF and Stuckenbruck S (1989), “Transients in liquid and structure in viscoelastic pipes,” *Proceedings of the 6th International Conference on Pressure Surges, BHRA*, Cambridge, UK, 69-84.
 76. Rachid FBF, Costa Mattos H, and Stuckenbruck S (1991), “Fluid-structure interaction in elasto-viscoplastic piping systems,” *Proceedings of the first ASME & JSME Joint Fluids Engineering Conference*, Portland, USA, ASME-FED **107** 65-73.
 77. Rachid FBF and Costa Mattos HS (1994), “Model for structural failure of elasto-viscoplastic pipelines,” *Meccanica* **29** 293-304.
 78. Rachid FBF, Costa Mattos H, and Stuckenbruck S (1992), “Waterhammer in inelastic pipes: an approach via an internal variable constitutive theory,” *Proceedings of the International Conference on Unsteady Flow and Fluid Transients*, Durham, UK, ISBN 90-5410-046-X, 63-70.
 79. Rachid FBF, Gama RMS, and Costa Mattos H (1994), “Modelling of hydraulic transients in damageable elasto-viscoplastic piping systems,” *Applied Mathematical Modelling* **18** 207-215.
 80. Rachid FBF and Costa Mattos HS (1995), “Pressure transients in damageable elasto-plastic pipes,” *Proceedings of the Joint ASME/JSME Pressure Vessels and Piping Conference*, Honolulu, USA, ASME-PVP **301** 31-40.
 81. Rachid FBF and Costa Mattos HS (1998), “Modelling of pipeline integrity taking into account the fluid-structure interaction,” *International Journal for Numerical Methods in Fluids* **28** 337-355.
 82. Rachid FBF and Costa Mattos HS (1999), “On the suitability of the low Mach number assumption in the modeling of the damage induced by pressure transients in piping systems,” *Journal of Fluids Engineering* **121** 112-117.
 83. Yu JH and Kojima E (1998), “Wave propagation in fluids contained in finite-length anisotropic viscoelastic pipes,” *Journal of the Acoustical Society of America* **104** 3227-3235.
 84. Suo L and Wylie EB (1990), “Complex wavespeed and hydraulic transients in viscoelastic pipes,” *Journal of Fluids Engineering* **112** 496-500.
 85. Paidoussis MP (1998), *Fluid-Structure Interactions (Slender Structures and Axial Flow)*, Vol. 1, Academic Press.
 86. Zhuge Q, Cai Y, and Yang S (1987), “Modal synthesis technique for vibration of complex piping systems,” *Proceedings of the first International Conference on Flow Induced Vibrations, BHRA*, Bowness-on-Windermere, UK, 513-520.
 87. Stittgen M and Zielke W (1989), “Fluid-structure interaction in flexible curved pipes,” *Proceedings of the 6th International Conference on Pressure Surges, BHRA*, Cambridge, UK,

101-120.

88. Piet-Lahanier N and Ohayon R (1990), "Finite element analysis of a slender fluid-structure system," *Journal of Fluids and Structures* **4** 631-645.
89. Dodds HL and Runyon HL (1965), "Effect of high velocity fluid flow on the bending vibrations and static divergence of a simply supported pipe," *NASA Technical Note D-2870*.
90. Davidson LC and Smith JE (1969), "Liquid-structure coupling in curved pipes," *The Shock and Vibration Bulletin*, No. 40, Part 4, 197-207.
91. Everstine GC (1984), "Dynamic analysis of fluid-filled piping systems using finite element techniques," *Advances in Fluid-Structure Interaction*, ASME-PVP **78**, ASME-AMD **64** 125-139.
92. Brown FT and Tentarelli SC (1988), "Analysis of noise and vibration in complex tubing systems with fluid-wall interactions," *Proceedings of the 43rd National Conference on Fluid Power*, Chicago, USA, 139-149.
93. Lee U, Pak CH, and Hong SC (1993), "Dynamics of piping system with internal unsteady flow," *Fluid-Structure Interaction, Transient Thermal-Hydraulics, and Structural Mechanics*, ASME-PVP **253** 103-110.
94. Païdoussis MP and Issid NT (1974), "Dynamic Stability of pipes conveying fluid," *Journal of Sound and Vibration* **33**(3) 267-294.
95. Lee U and Kim J (1999), "Dynamics of branched pipeline systems conveying internal unsteady flow," *Journal of Vibration and Acoustics* **121** 114-122.
96. Wang Z-M and Tan SK (1997), "Coupled analysis of fluid transients and structural dynamic responses of a pipeline system," *Journal of Hydraulic Research* **35** 119-131.
97. Wang Z-M and Tan SK (1998), "Vibration and pressure fluctuation in a flexible hydraulic power system on an aircraft," *Computers & Fluids* **27** 1-9.
98. Clough RW and Penzien J (1975), *Dynamics of Structures*, McGraw-Hill.
99. Weaver W, Timoshenko SP, and Young DH (1990), *Vibration Problems in Engineering* (5th edition), John Wiley and Sons.
100. Vardy AE and Alsarraj AT (1991), "Coupled axial and flexural vibration of 1-D members," *Journal of Sound and Vibration* **148** 25-39.
101. Fan D (1989), "Fluid-structure interactions in internal flows," Ph.D. Thesis, The University of Dundee, Department of Civil Engineering, Dundee, UK.
102. Valentin RA, Phillips JW, and Walker JS (1979), "Reflection and transmission of fluid transients at an elbow," *Transactions of SMiRT5*, Berlin, Germany, Paper B 2/6.
103. Hsu CK and Phillips JW (1981), "Pulse propagation in fluid-filled elastic curved tubes," *Journal of Pressure Vessel Technology* **103** 43-49.
104. Chen SS (1972), "Flow-induced in-plane instabilities of curved pipes," *Nuclear Engineering and Design* **23** 29-38.
105. Chen SS (1973), "Out-of-plane vibration and stability of curved tubes conveying fluid," *Journal of Applied Mechanics* **40** 362-368.
106. Dupuis C and Rousselet J (1992), "The equations of motion of curved pipes conveying fluid," *Journal of Sound and Vibration* **153**(3) 473-489.
107. Dodge WG and Moore SE (1972), "Stress indices and flexibility factors for moment loadings on elbows and curved pipe," *Welding Research Council Bulletin* **179**.
108. Leslie DJ and Tijsseling AS (1999), "A review of modelling damping mechanisms in coupled liquid-pipe vibrations," *Proceedings of the 3rd ASME & JSME Joint Fluids Engineering Conference, Symposium S-290 Waterhammer* (Editor JCP Liou), San Francisco, USA, ASME-FED **248** 1-8.
109. Budny DD, Hatfield FJ, and Wiggert DC (1990), "An experimental study on the influence of

- structural damping on internal fluid pressure during a transient flow," *Journal of Pressure Vessel Technology* **112** 284-290.
110. Budny DD, Wiggert DC, and Hatfield FJ (1991), "The influence of structural damping on internal pressure during a transient flow," *Journal of Fluids Engineering* **113** 424-429.
111. Leslie DJ and Tijsseling AS (1999), "Wave speeds and phase velocities in liquid-filled pipes," *Proceedings of the 9th International Meeting of the IAHR Work Group on the Behavior of Hydraulic Machinery under Steady Oscillatory Conditions*, Brno, Czech Republic, Paper E1.
112. Kruisbrink ACH (1990), "Modelling of safety and relief valves in waterhammer computer codes," *Proceedings of the 3rd International Conference on Developments in Valves and Actuators for Fluid Control*, BHRA, Bournemouth, UK, 137-149.
113. Wylie EB (1984), "Simulation of vaporous and gaseous cavitation," *Journal of Fluids Engineering* **106** 307-311.
114. Zielke W and Perko H-D (1985), "Low pressure phenomena and waterhammer analysis," *3R international* **24** 348-355 (in German).
115. Fan D and Tijsseling AS (1992), "Fluid-structure interaction with cavitation in transient pipe flows," *Journal of Fluids Engineering* **114** 268-274.
116. Tijsseling AS, Vardy AE, and Fan D (1996), "Fluid-structure interaction and cavitation in a single-elbow pipe system," *Journal of Fluids and Structures* **10** 395-420.
117. Hatfield FJ and Wiggert DC (1991), "Waterhammer response of flexible piping by component synthesis," *Journal of Pressure Vessel Technology* **113** 115-119.
118. Mansour SGS (1998), "Waterhammer and fluid-structure interaction modelling," Ph.D. Thesis, Technical University Braunschweig, Department of Civil Engineering, Leichtweiss Institute for Hydraulic Engineering, Braunschweig, Germany.
119. Mansour SGS (1998), "The application of Verwey-Yu scheme in FSI simulations," *Proceedings of the 3rd International Conference on Hydroinformatics*, Copenhagen, Denmark.
120. Abbott MB and Basco DR (1989), *Computational Fluid Dynamics. An Introduction for Engineers*, Longman.
121. Greenshields CJ, Weller HG, and Ivankovic A (1999), "The finite volume method for coupled fluid flow and stress analysis," *Computer Modeling and Simulation in Engineering* **4** 213-218.
122. Bahrar B, Rieutord E, Morel R, and Zeggwagh G (1998), "Modeling of the waterhammer phenomenon with respect to real pipe behavior," *La Houille Blanche - Revue Internationale de l'Eau* **53** 18-25 (in French).
123. Tijsseling AS and Lavooij CSW (1990), "Waterhammer with fluid-structure interaction," *Applied Scientific Research* **47** 273-285.

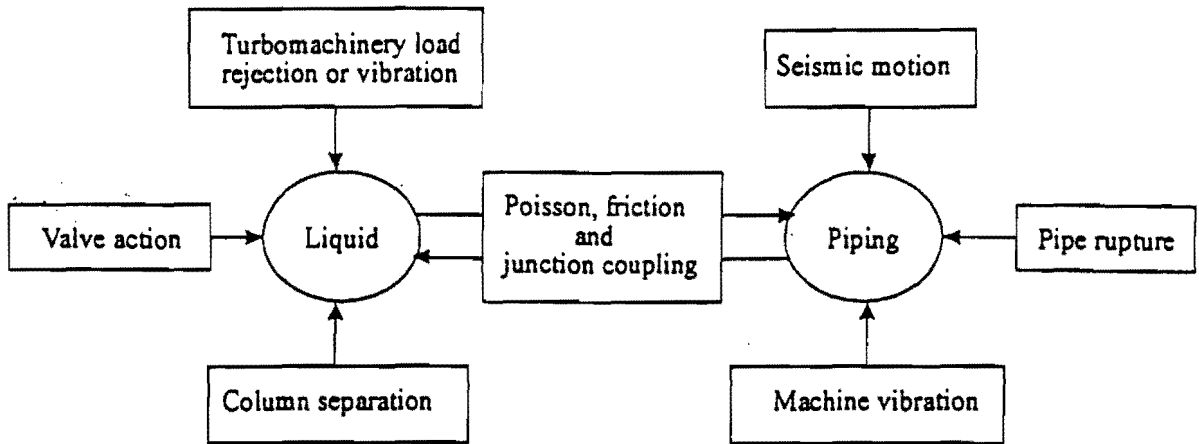
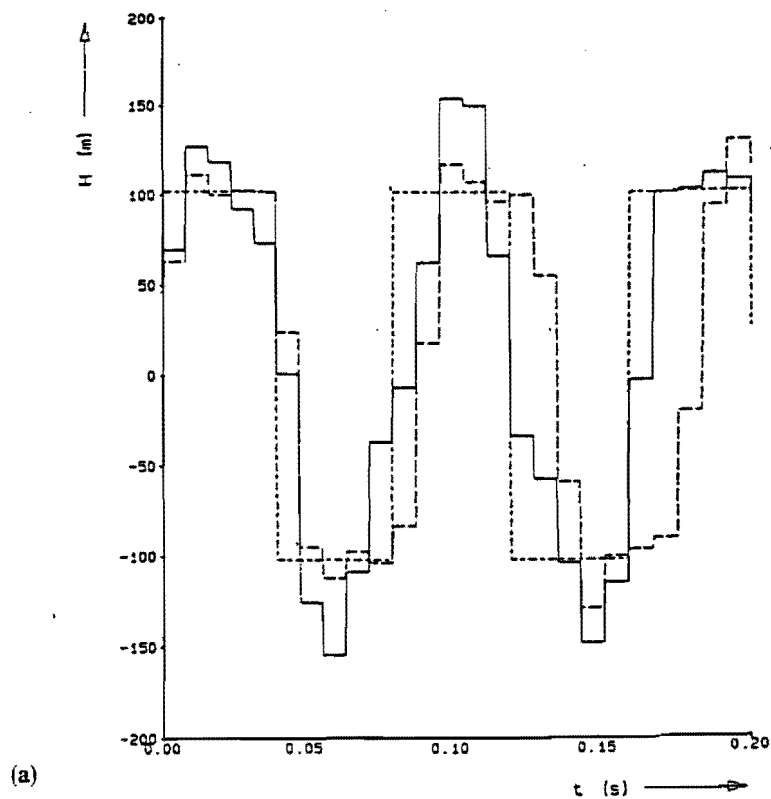
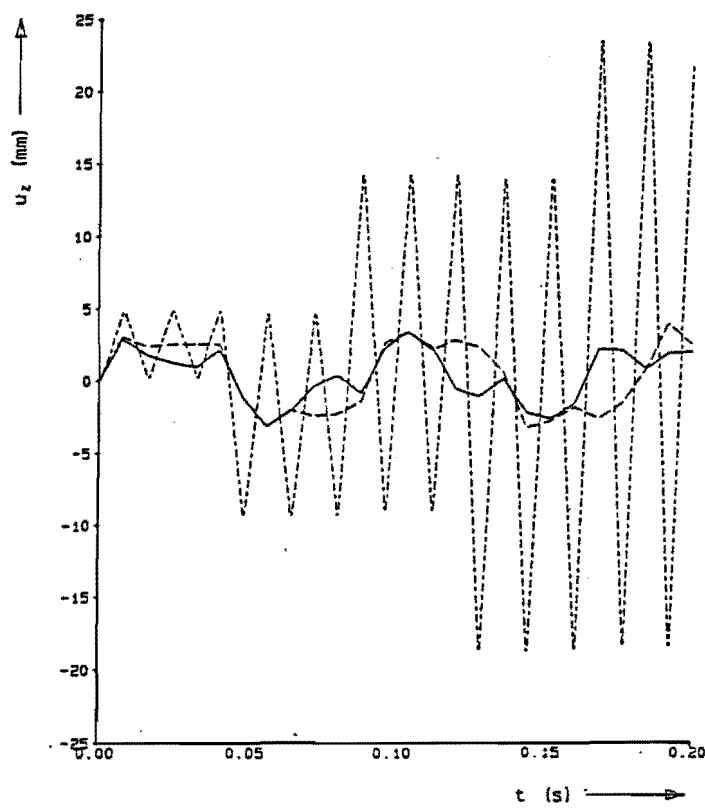


FIGURE 1.

Sources of excitation and interaction between liquid and piping.



(a)



(b)

FIGURE 2.

Instantaneous closure of unrestrained valve in reservoir-pipe-valve-system: (a) pressure head at valve; (b) axial displacement of valve. Uncoupled (dotted line), junction coupling (dashed line), Poisson and junction coupling (solid line) [Tijsseling and Lavooij, 123].

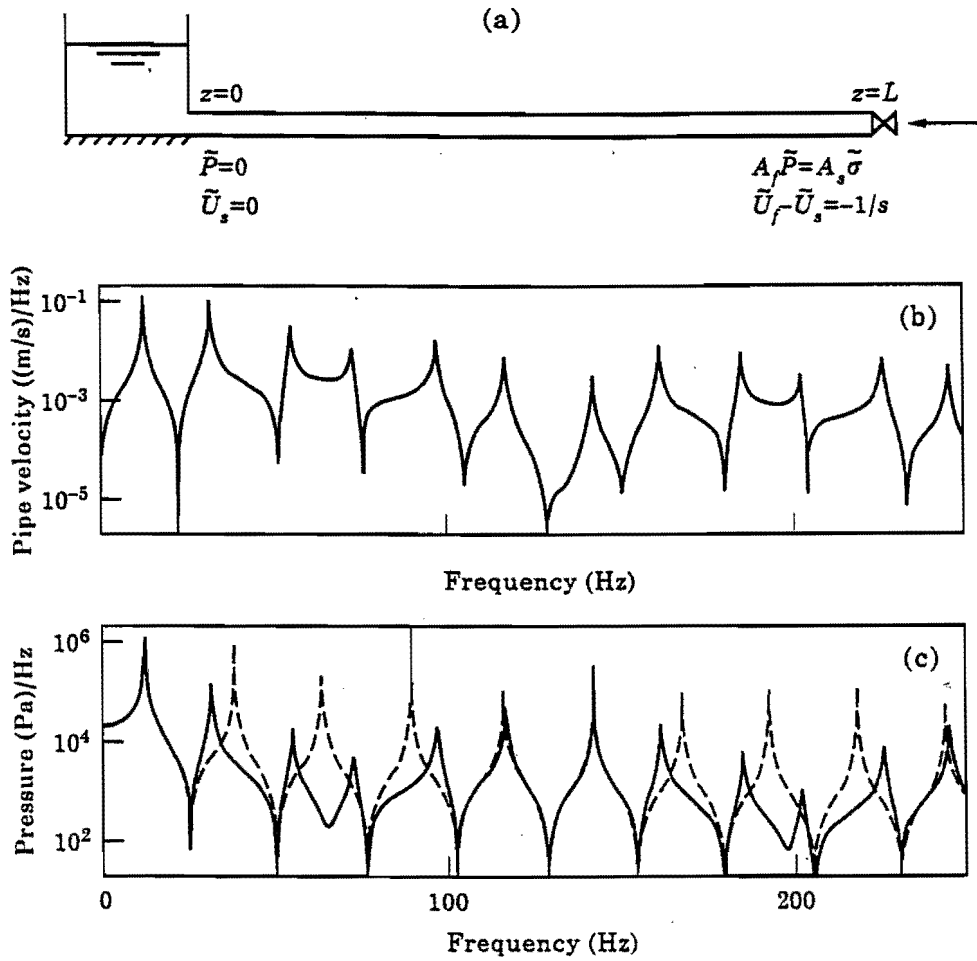


FIGURE 3.

Instantaneous closure of unrestrained valve in reservoir-pipe-valve-system: (a) boundary conditions in frequency domain; (b) axial pipe velocity spectra; (c) pressure spectra, with FSI (solid line), without FSI (broken line) [Zhang et al, 35].

PRESSURE TIME HISTORY AT VALVE
 RE=1900 DAMPING =1%

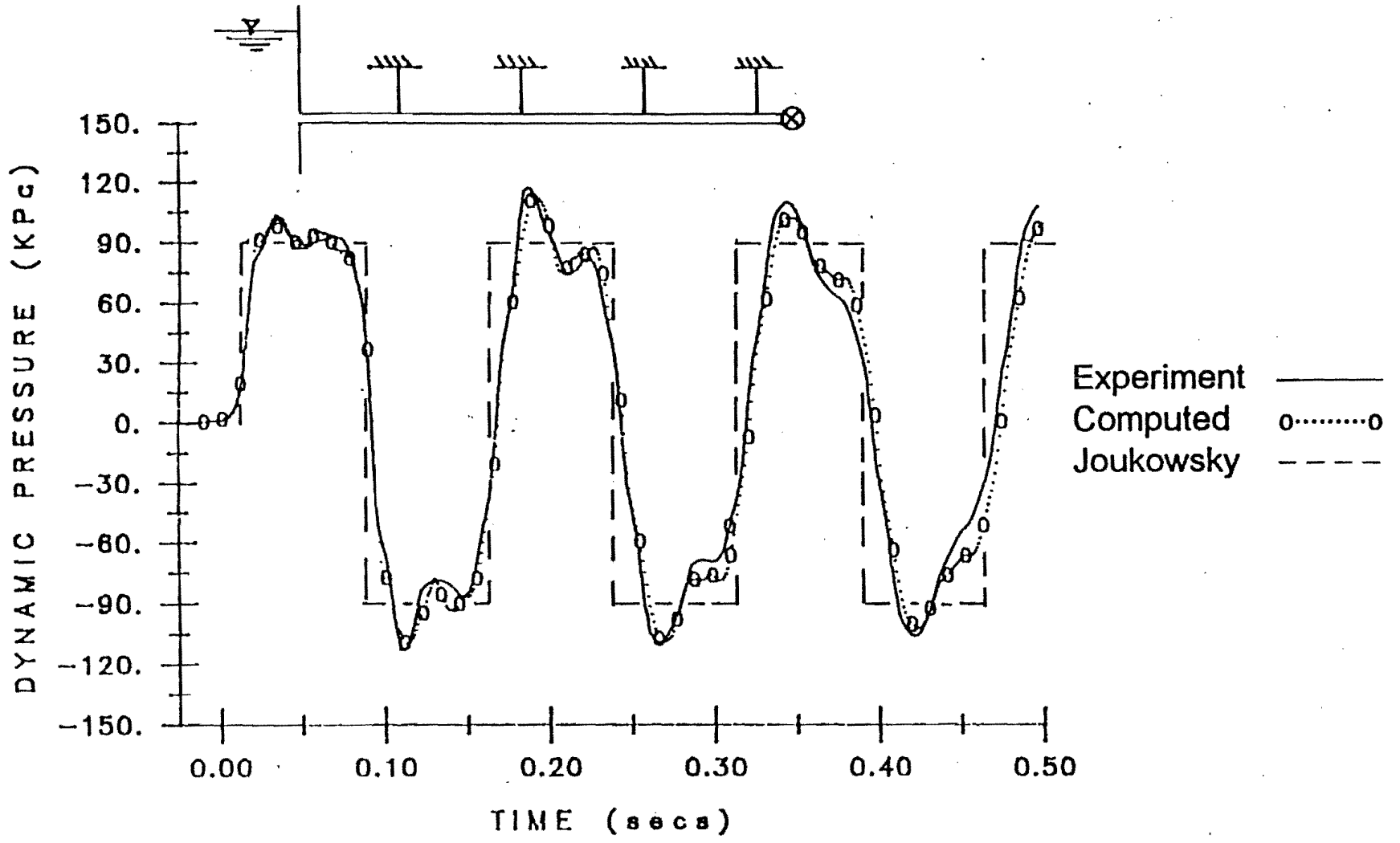


FIGURE 4.

Instantaneous closure of unrestrained valve in reservoir-pipe-valve-system:
 pressure time history at valve [Wiggert, 3].

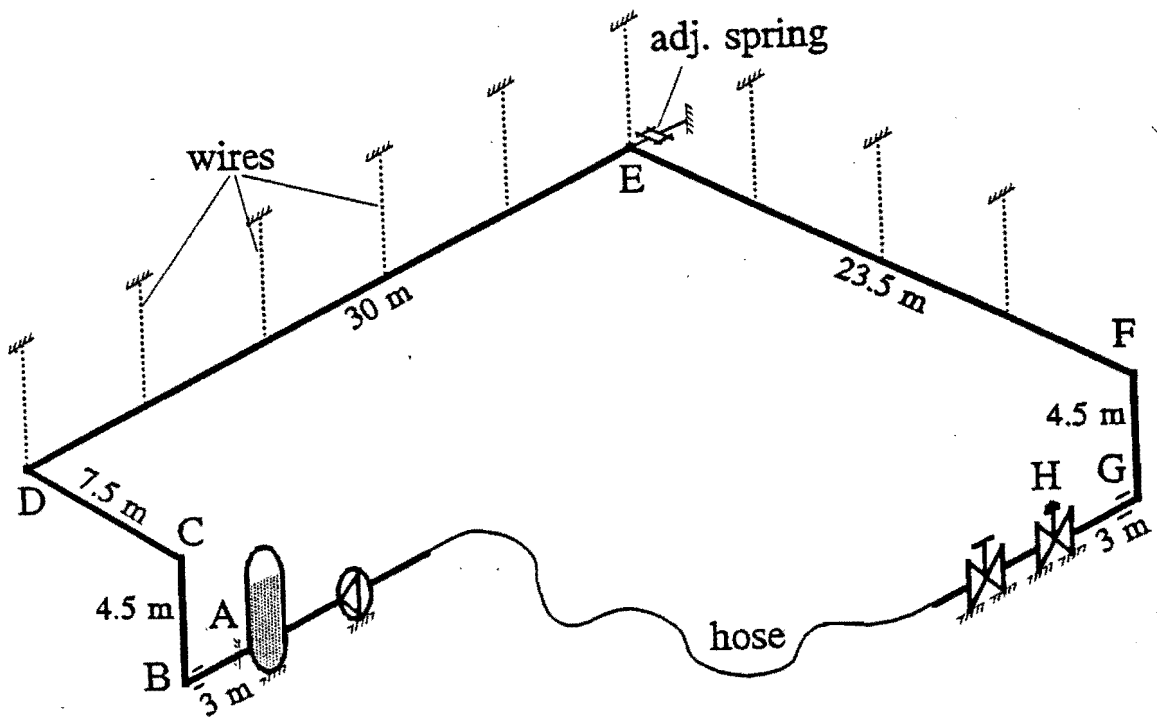


FIGURE 5.

Instantaneous closure of valve in reservoir-pipe-valve-system: tested and simulated pipeline system [Kruisbrink and Heinsbroek, 12].

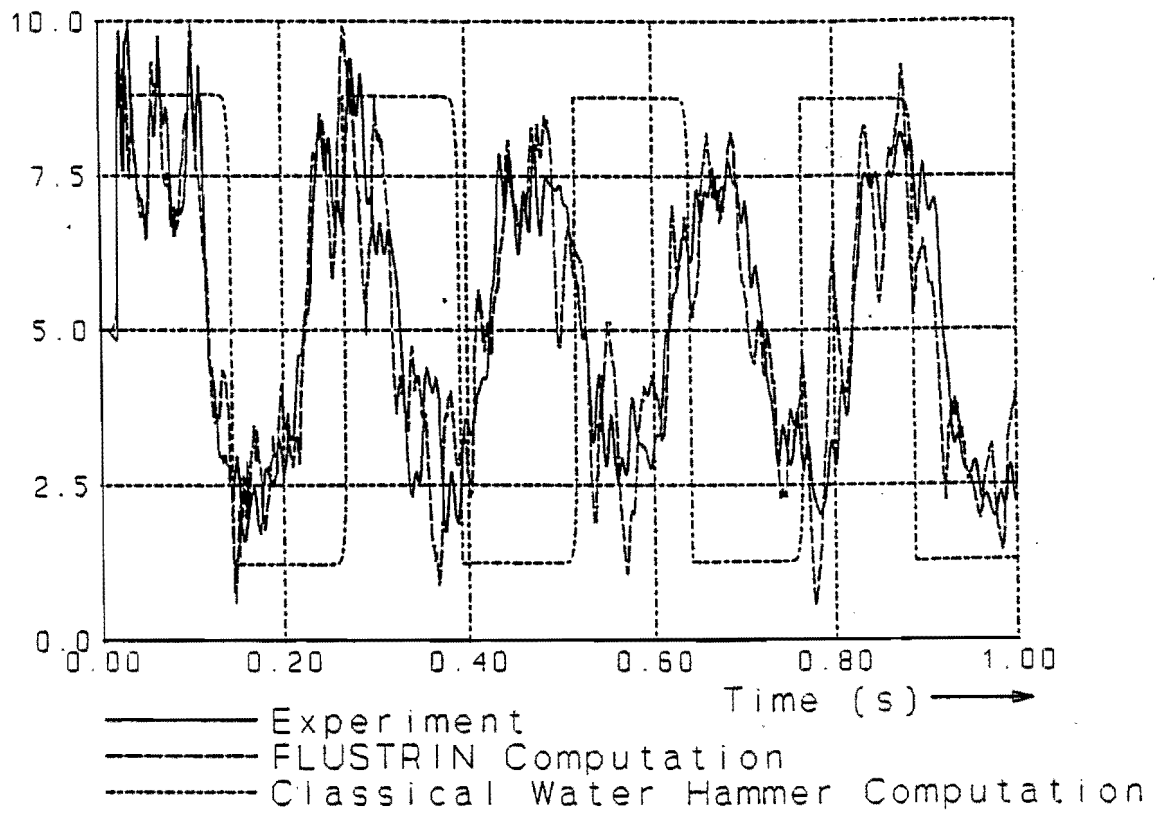


FIGURE 6A.

Instantaneous closure of valve in reservoir-pipe-valve-system:(a) measured and computed dynamic pressure near the shut-off valve [Kruisbrink and Heinsbroek, 12].

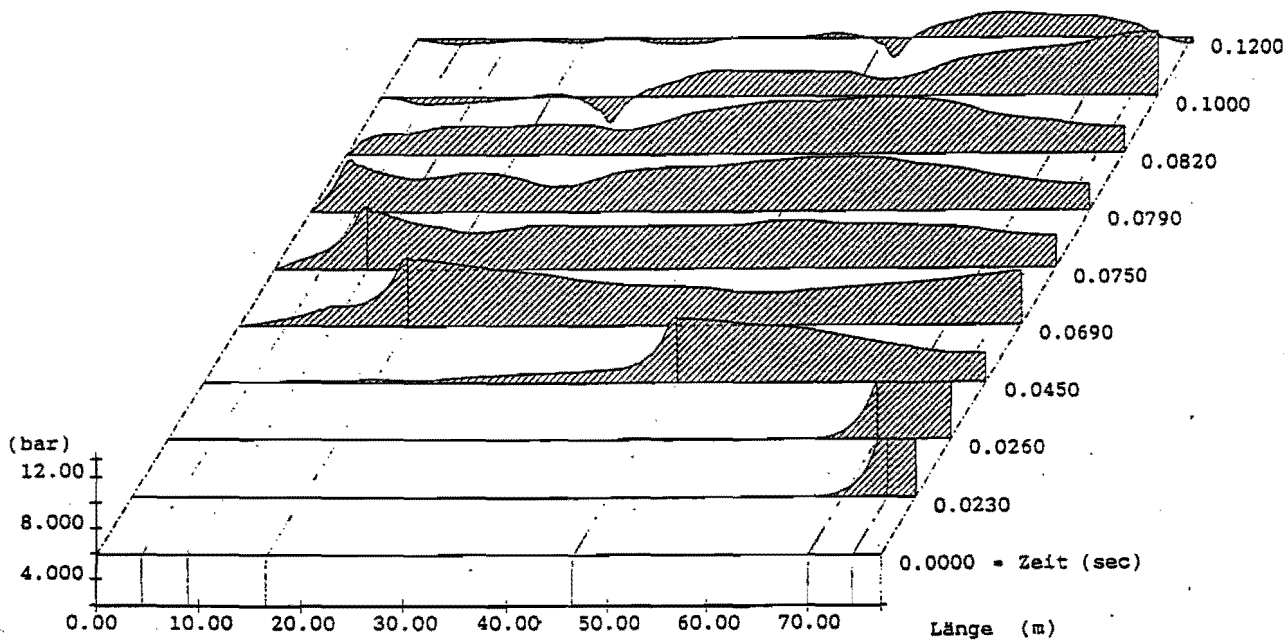
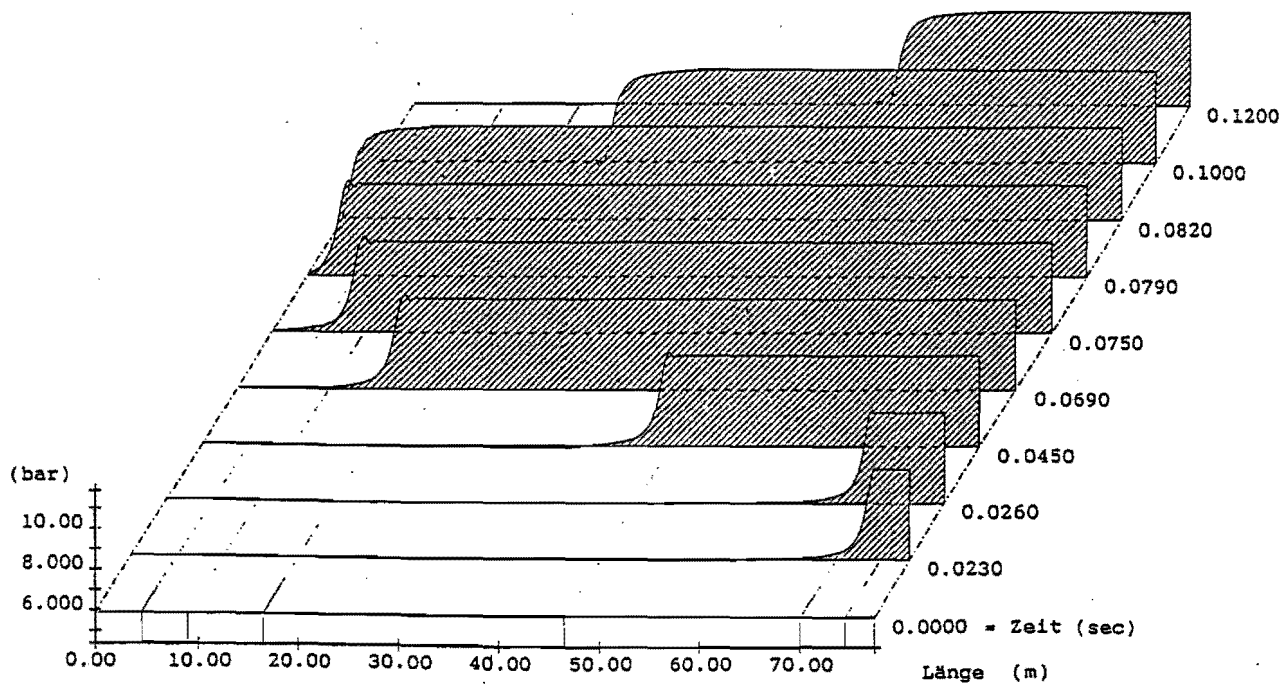


FIGURE 6B.

Instantaneous closure of valve in reservoir-pipe-valve-system: computed pressure waveforms in the time-distance plane without FSI (upper) and with FSI (lower) [Enkel and Grams, 13].

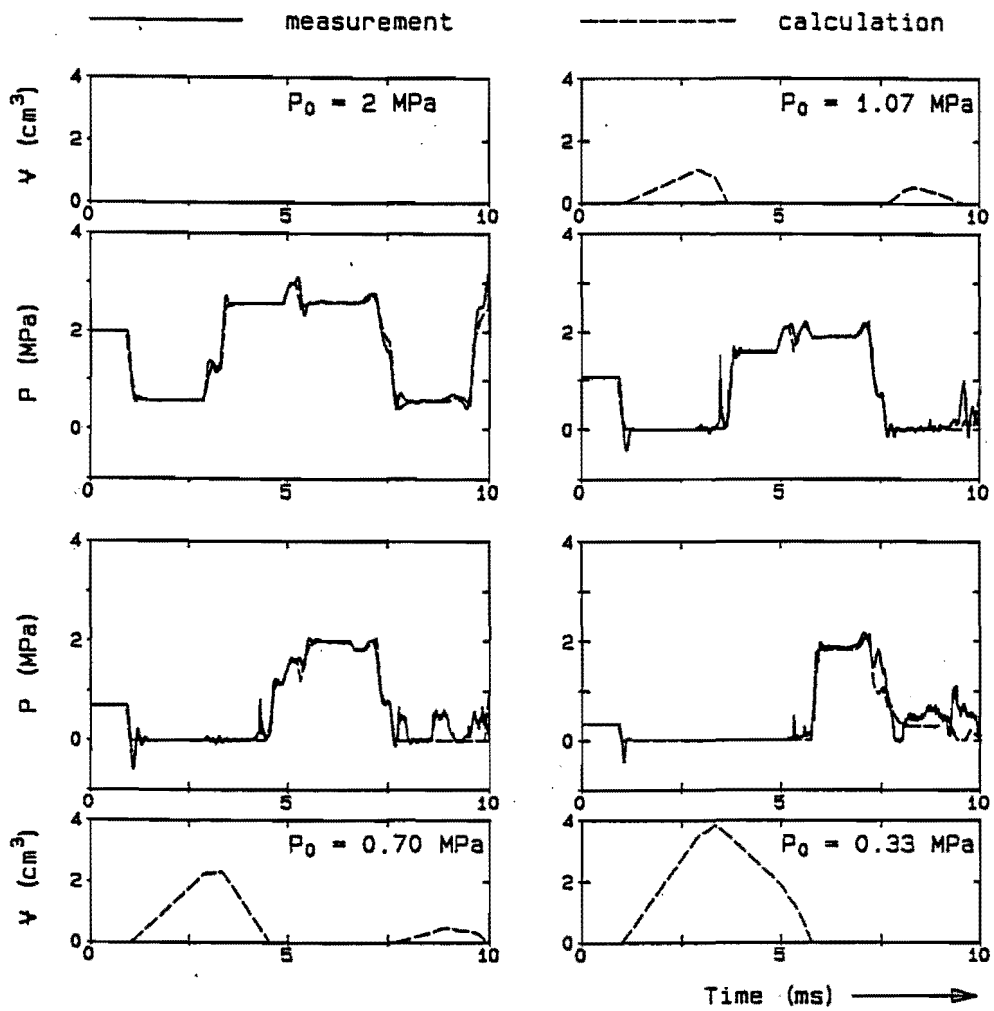


FIGURE 7.

Moving water-filled pipe with column separation: experimental and theoretical results [Tijsseling and Fan, 14].

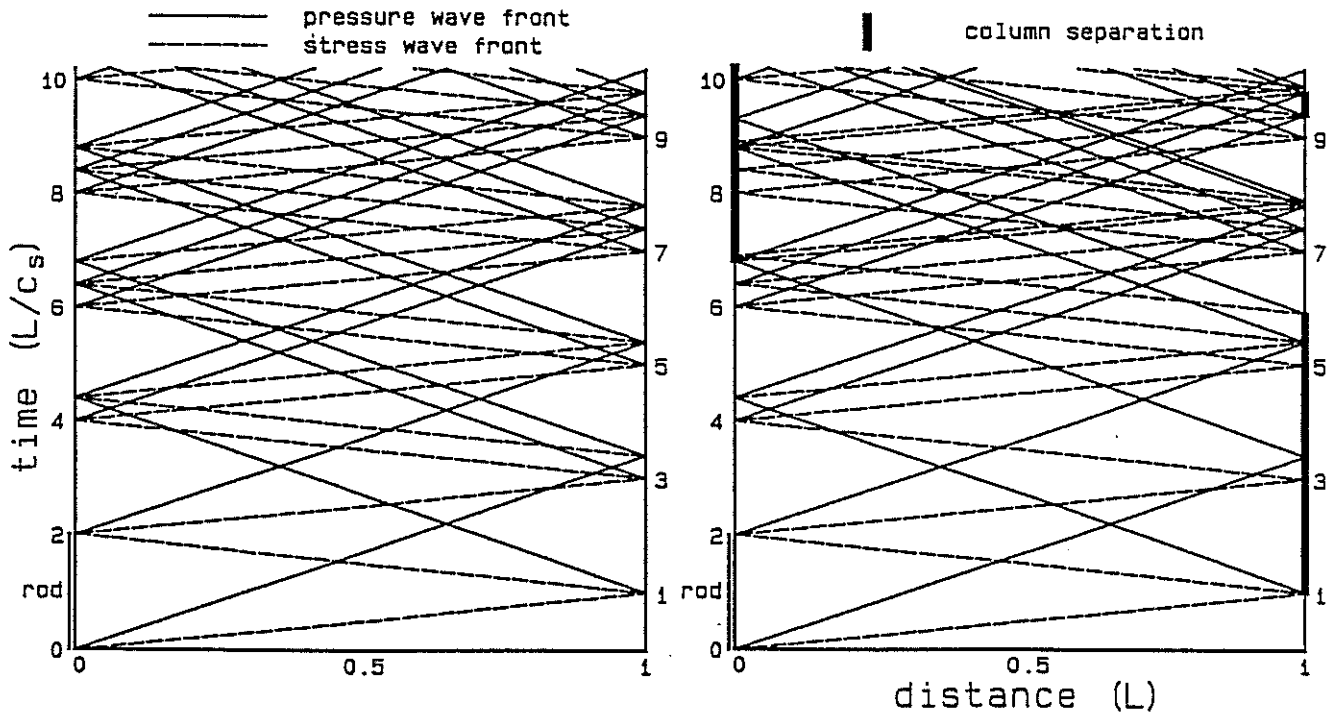
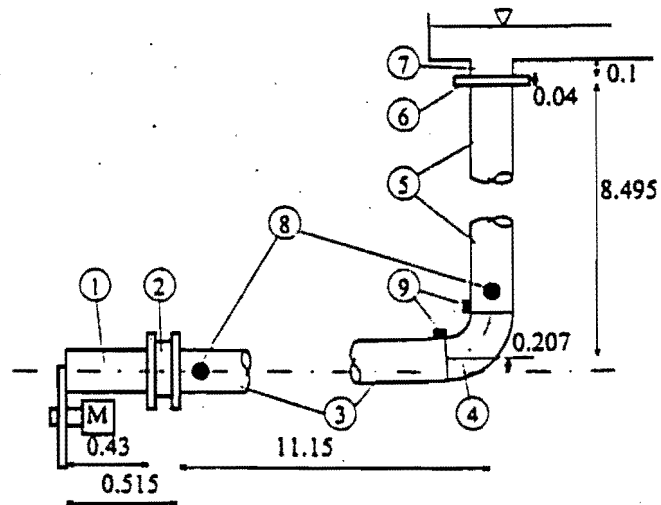


FIGURE 8.

Moving water-filled pipe with column separation: wave paths in distance-time diagram [Tijsseling and Fan, 14].



Number	Dimension	mm	Description [SI units]
1	D100, d80		Stainless steel, $\rho = 7840$, $E = 2.0 * 10^{11}$, $\nu = 0.3$
2	D \approx 200, d80		Shutdown valve, bolted between DIN 2576 80 PN10 flanges
3	D83, d80		Stainless steel, $\rho = 7840$, $E = 2.0 * 10^{11}$, $\nu = 0.3$
4	D84, d80, R130		Bend, stainless steel, $\rho = 7840$, $E = 2.0 * 10^{11}$, $\nu = 0.3$
5	D83, d80		Stainless steel, $\rho = 7840$, $E = 2.0 * 10^{11}$, $\nu = 0.3$
6	D200, d80		DIN 2576 80 PN10 flange and steel flange 80 PN 10
7	D100, d80		Steel, $\rho = 7840$, $E = 2.1 * 10^{11}$, $\nu = 0.3$
8	-		Entran pressure transducer
9	-		Entran accelerometer

FIGURE 9.

Experimental piping system: (upper) schematic: dimensions are in meters; (lower) dimensions and material properties of the system: D and d are outer and inner diameters [Svingen, 21].

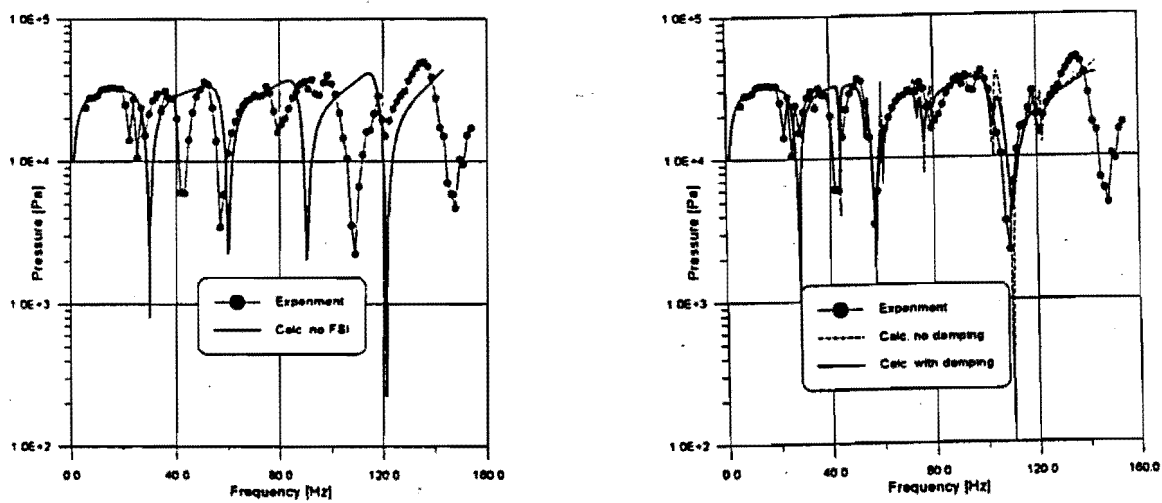


FIGURE 10.

Pressure spectra at valve: (left) calculations without FSI, without damping; (right) calculations with FSI, with damping, and without damping [Svingen, 21].

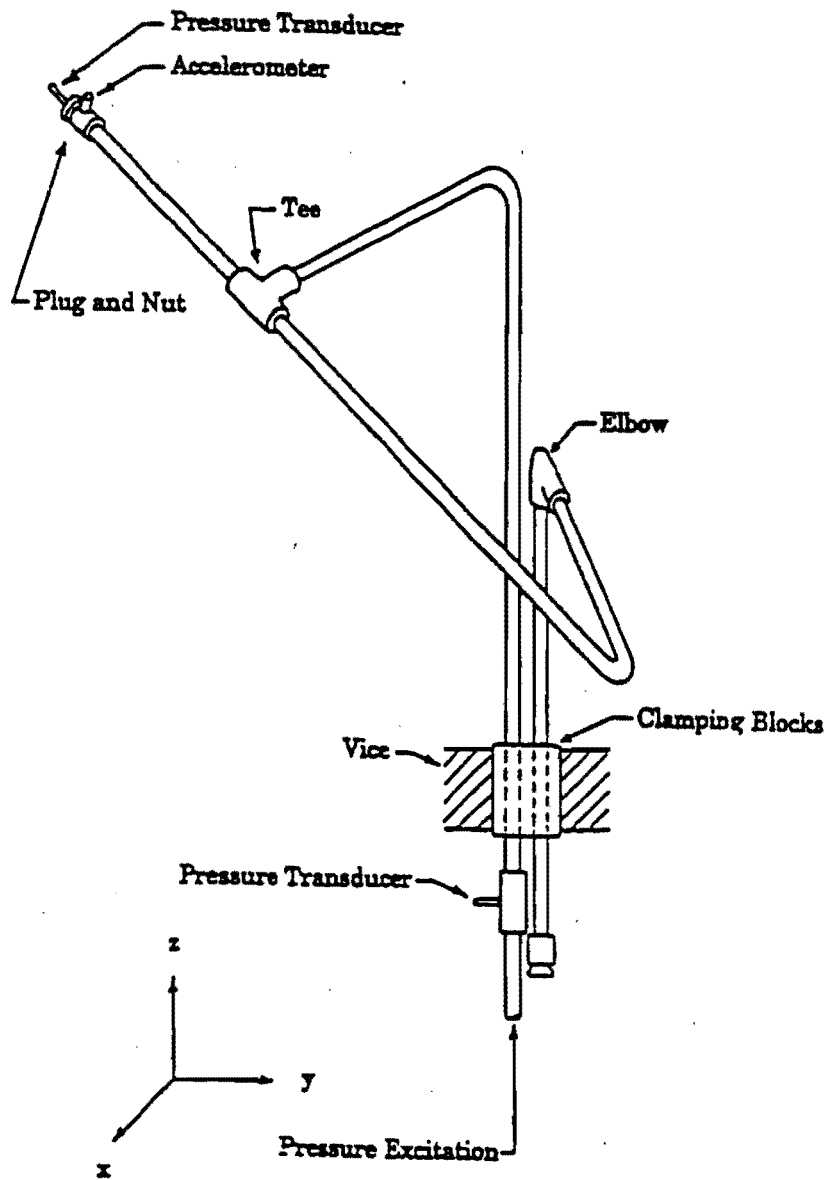


FIGURE 11A.

Complex system: schematic of the experiment [Tentarelli, 16, and Tentarelli and Brown, 18].

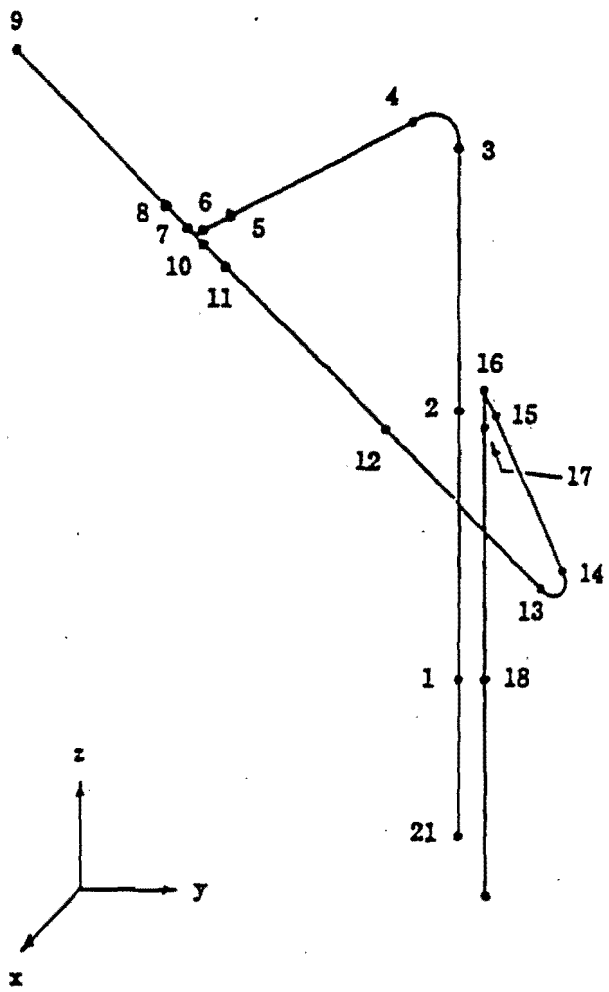


FIGURE 11B.

Complex system: node diagram used in calculation [Tentarelli, 16, and Tentarelli and Brown, 18].

Case A: Closed-end at Node 19

Fluid density	835.16 kg/m ³
Fluid bulk modulus	1.606 x 10 ⁹ Pa
Kinematic viscosity	3.0 x 10 ⁻⁵ m ² /sec
Fluid Temperature	23.3° C
Wall density	7870. kg/m ³
Young's modulus	2.07 x 10 ¹¹ Pa
Poisson's ratio	0.29
Material loss coefficient η	0.001
Inside pipe radius	5.13 mm
Outside pipe radius	6.325 mm <i>between nodes 1-5, 8-9, 11-15, 17-18</i>
Outside pipe radius	10.36 mm <i>between nodes 6-6, 7-8, 10-11</i>
Outside pipe radius	10.51 mm <i>between nodes 15 - 17</i>
Outside pipe radius	17.0 mm <i>between nodes 21 - 1, 18 - 19</i>
Radius of bends	39.4 mm
Ovalization ratio	1.110 <i>between nodes 3 - 4, 13 - 14</i>

The node coordinates in meters are:

Node	x	y	z
1	0.0	0.0	0.0
2	0.0	0.0	0.5551
3	0.0	0.0	1.1101
4	0.0323	-0.0028	1.1484
5	0.3369	-0.0294	1.1996
6	0.3743	-0.0328	1.2059
7	0.3743	-0.0328	1.2059
8	0.3673	-0.0537	1.2369
9	0.2958	-0.2665	1.5517
10	0.3743	-0.3275	1.2059
11	0.3814	-0.0118	1.1749
12	0.4567	0.2125	0.8432
13	0.5321	0.4367	0.5112
14	0.4929	0.4310	0.4572
15	0.0294	0.0496	0.4572
16	0.0	0.0254	0.4572
17	0.0	0.0254	0.4191
18	0.0	0.0254	0.0
19	0.0	0.0254	-0.1828
21	0.0	0.0	-0.2466

The boundary conditions and lumped impedances are:

- node 21 Cantilevered end with pressure excitation.
- node 1 Rigidly clamped.
- node 6 $I_x, I_y, I_z = 3.0 \times 10^{-5} \text{ kg-m}^2$.
- node 9 Free-end, closed-end, mass = 0.083 kg, $I_x = 1.73 \times 10^{-5} \text{ kg-m}^2$,
 $I_y = 1.7 \times 10^{-5} \text{ kg-m}^2$, $I_z = 5.0 \times 10^{-5} \text{ kg-m}^2$.
- node 16 $I_x, I_y, I_z = 2.6 \times 10^{-5} \text{ kg-m}^2$.
- node 18 Rigidly clamped.
- node 19 Free-end, closed-end, mass = 0.08 kg.

The total mass at node 9 due to the plug, nut, ferulok, pressure transducer, and accelerometer is 0.083 kg. The large radius between nodes 5-6, 7-8, and 10-11 accounts for the mass of the tee, increases the pipe stiffness and adds some rotary inertia. Some additional inertia is also added at node 6 as noted above. The large radius between nodes 15-17 accounts for the mass of the elbow, increases the pipe stiffness, and adds some rotary inertia. Some additional inertia is also added at node 16 as noted above. The large radius between nodes 18-19 and 21-1 accounts for the stiffening effect of the transducer mounting block and the vice.

FIGURE 11C.
Complex system: experiment parameters [Tentarelli, 16, and Tentarelli and Brown, 18].

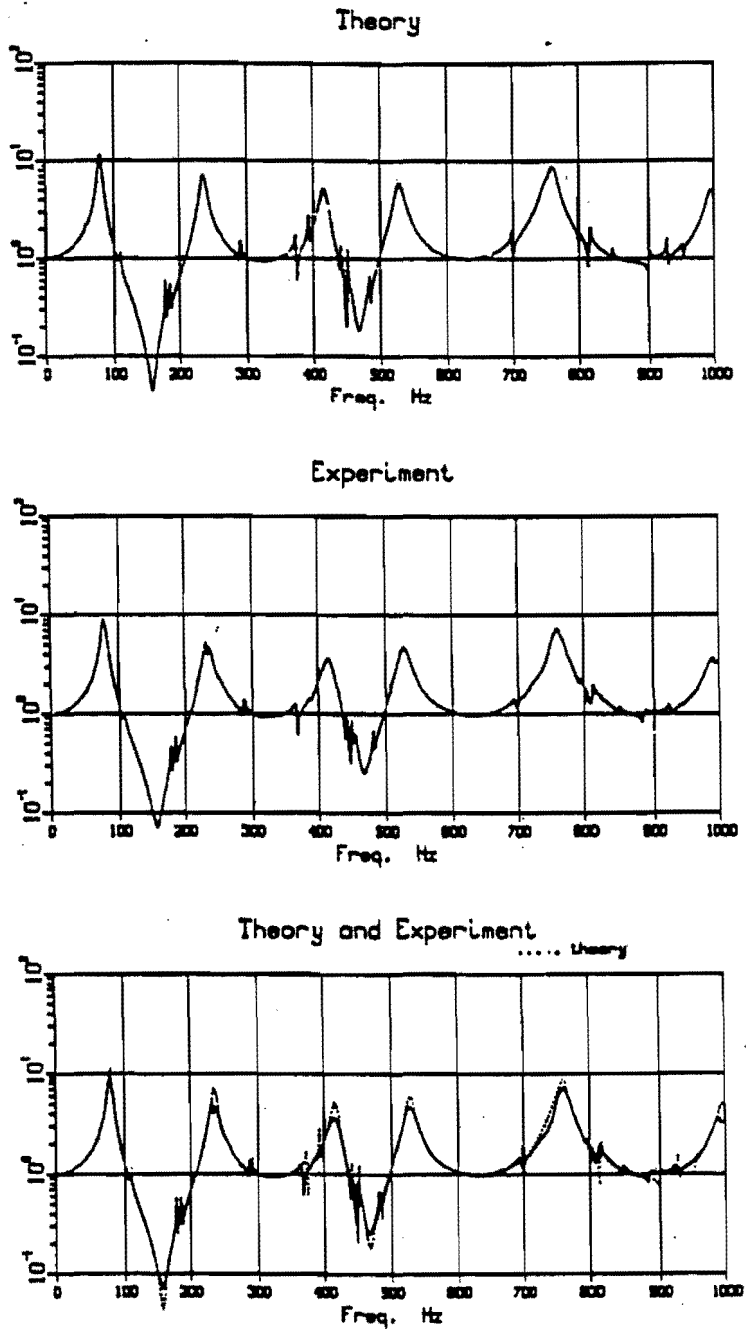
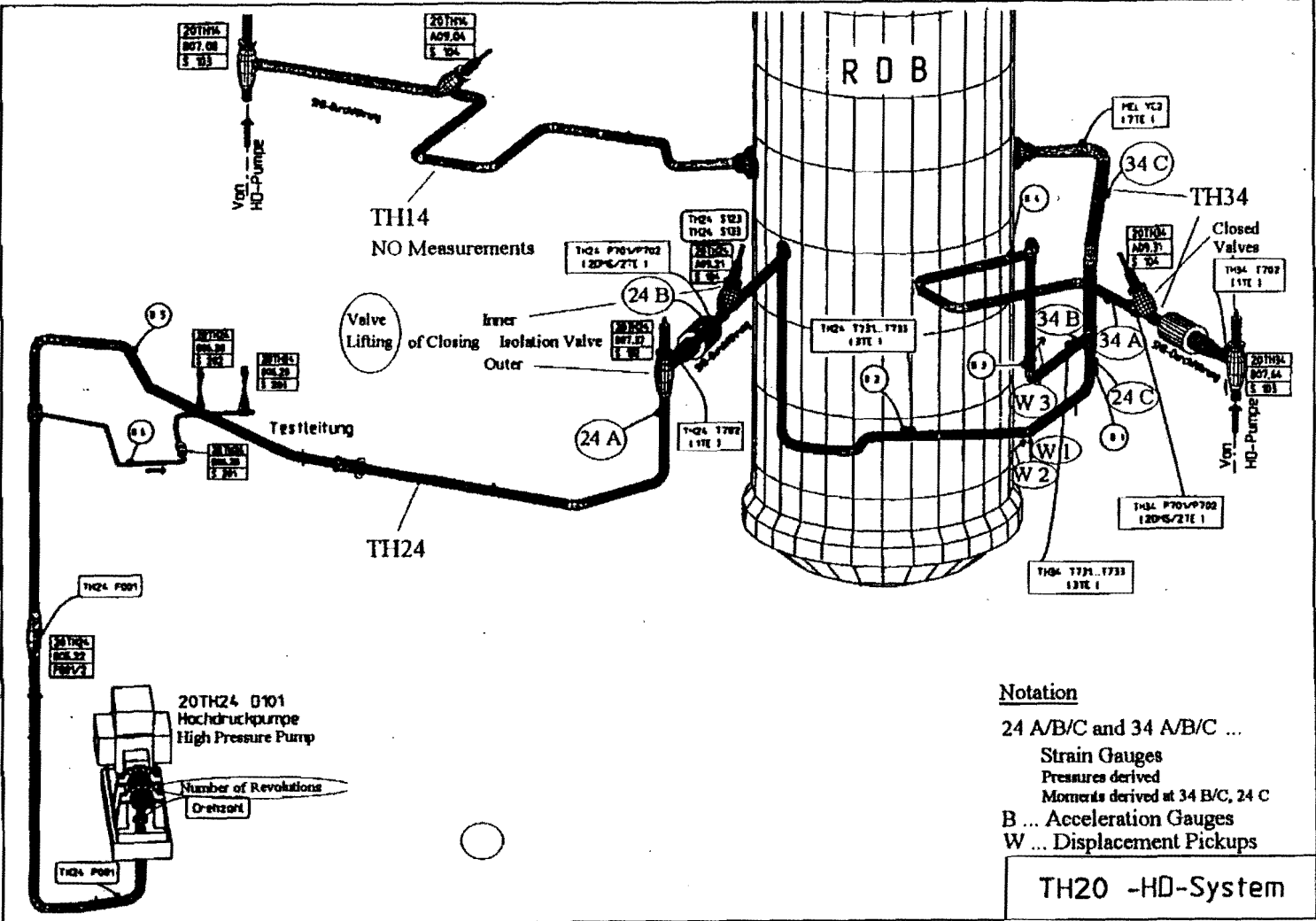


FIGURE 12.

Pressure spectra at free closed end divided by the pressure excitation spectra: Comparison between theory and experiment. The ordinate is the pressure at the free closed end divided by the excitation pressure [Tentarelli, 16, and Tentarelli and Brown, 18].



Notation
 24 A/B/C and 34 A/B/C ...
 Strain Gauges
 Pressures derived
 Moments derived at 34 B/C, 24 C
 B ... Acceleration Gauges
 W ... Displacement Pickups

TH20 -HD-System

FIGURE 13A.

Nuclear piping system: layout [Erath et al, 39].

Notation: 24 A/B/C and 34 A/B/C ... Strain Gauges
 at 24 A/B/C, 34 A/B/C ... Pressures Derived
 at 24 C, 34 B and 34 C ... Moments Derived
 W1, W2, W3 ... Displacement Pickups
 B 1 - B 6 ... Acceleration Gauges

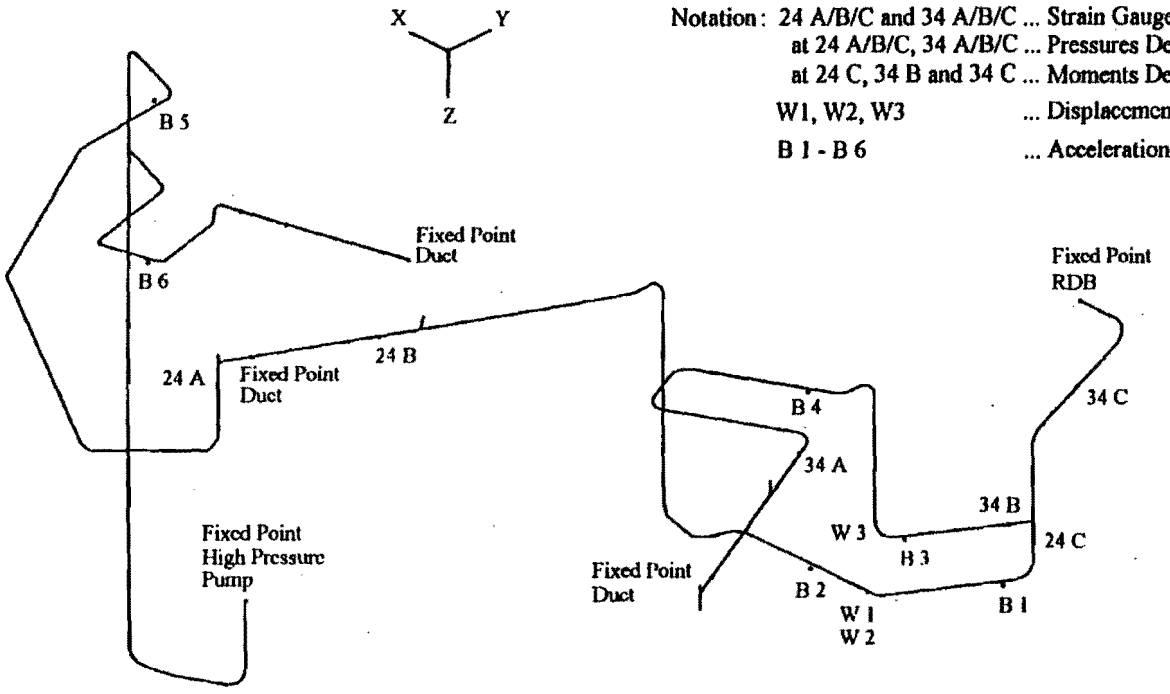


FIGURE 13B.

Nuclear piping system: structural model [Errath et al, 39].

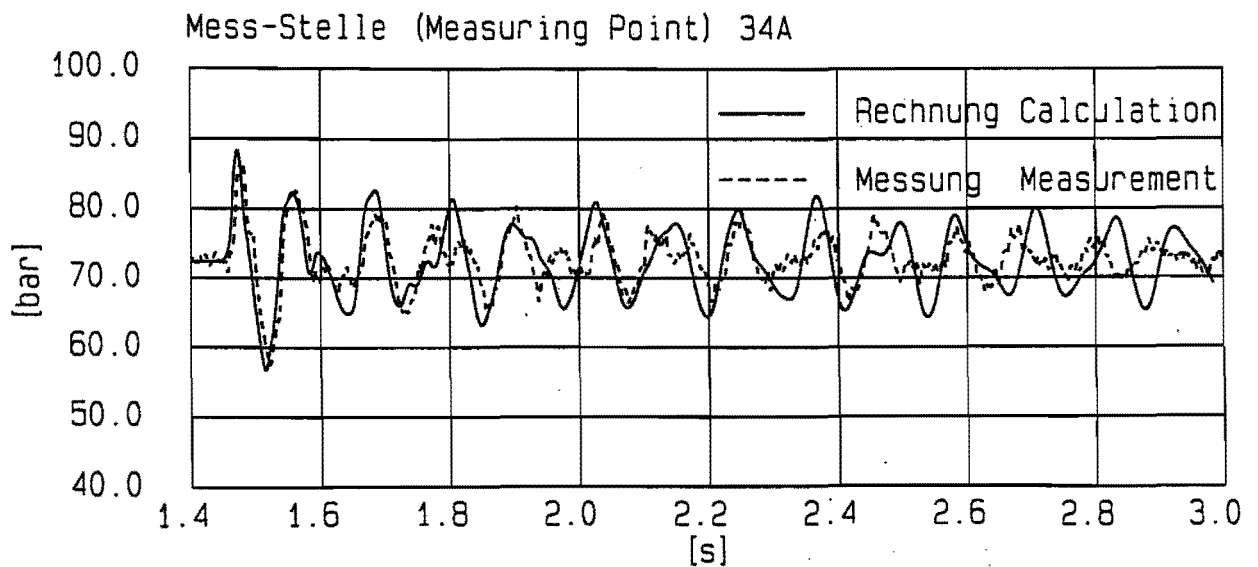
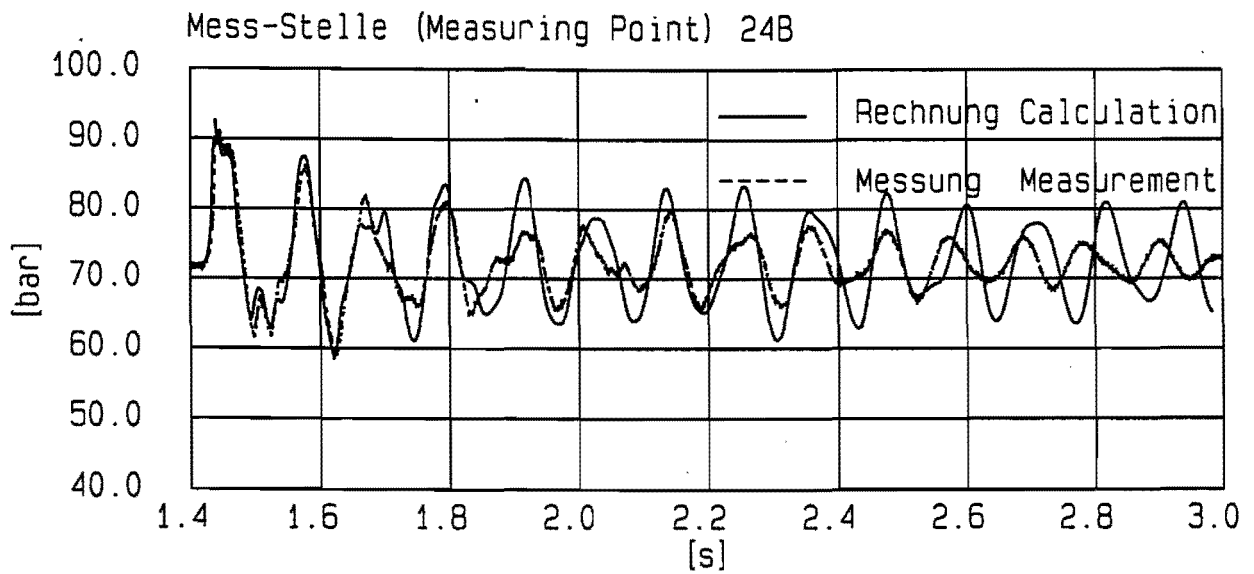
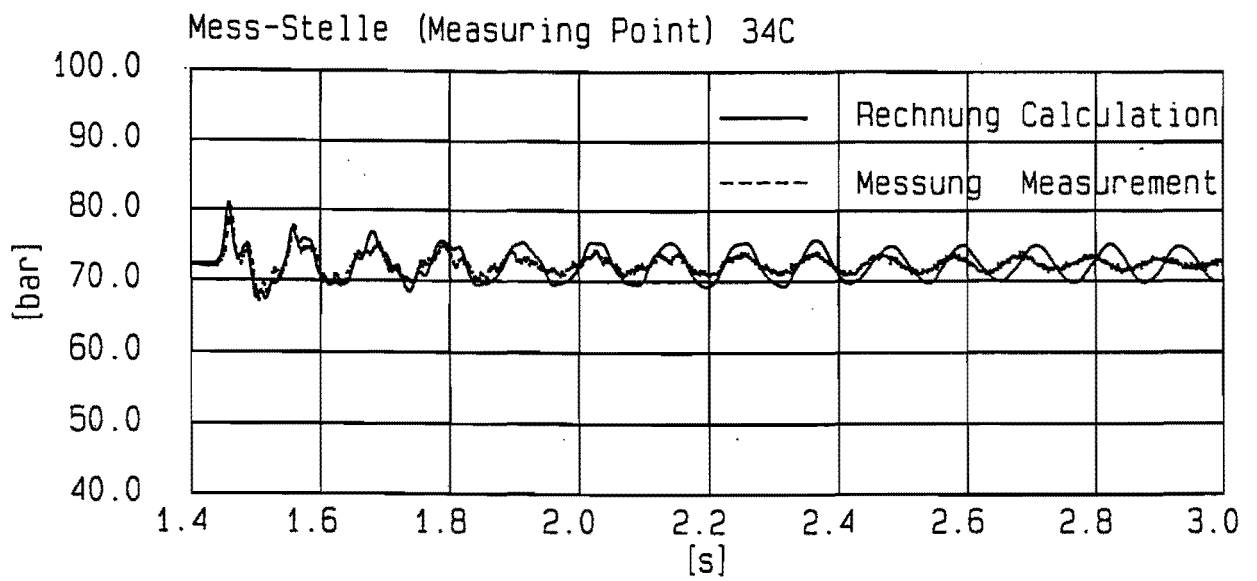
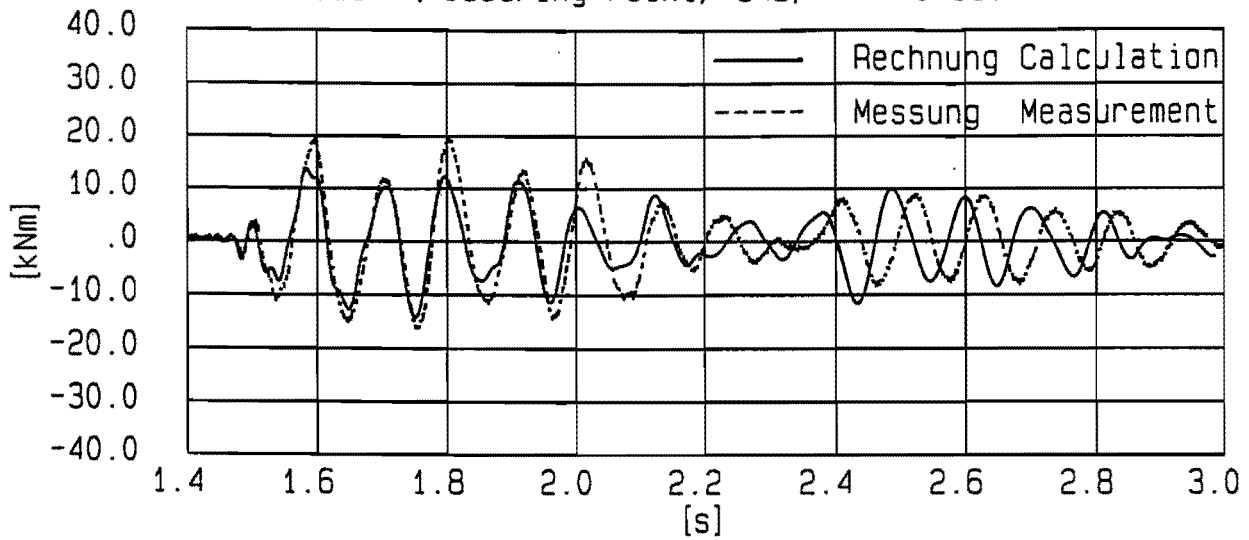


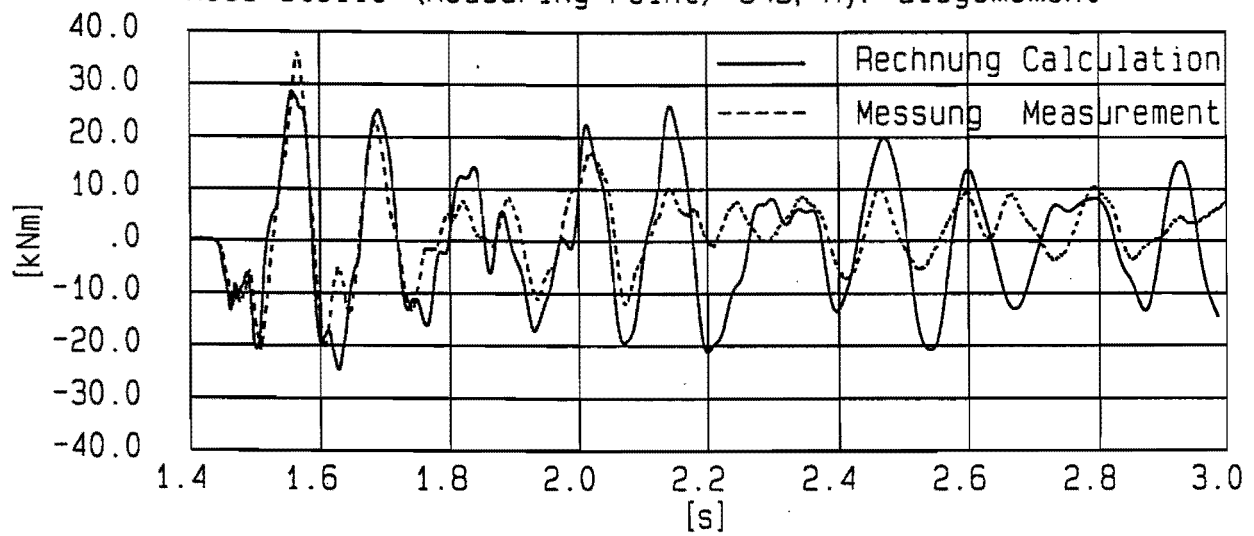
FIGURE 14A.

Pump shutdown with valve closure in nuclear piping system: comparisons between calculation (solid line) and measurement (broken line): pressures [Erath et al, 38].

Mess-Stelle (Measuring Point) 34B; Mx: Torsionsmoment



Mess-Stelle (Measuring Point) 34B; My: Biegemoment



Mess-Stelle (Measuring Point) 34B; Mz: Biegemoment

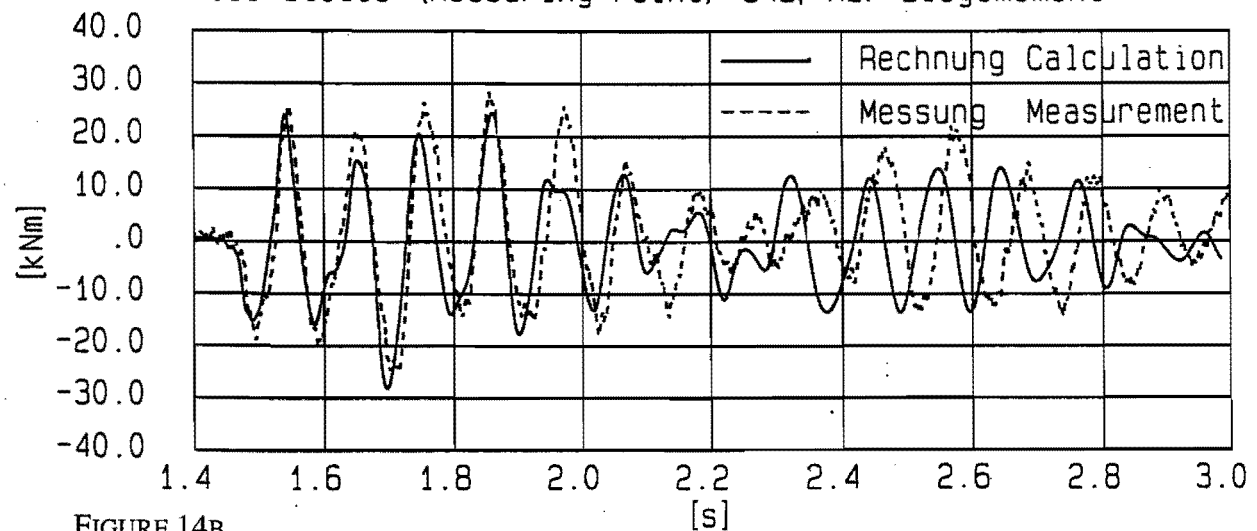


FIGURE 14B.

Pump shutdown with valve closure in nuclear piping system: comparisons between calculation (solid line) and measurement (broken line): moments [Erath et al, 38].

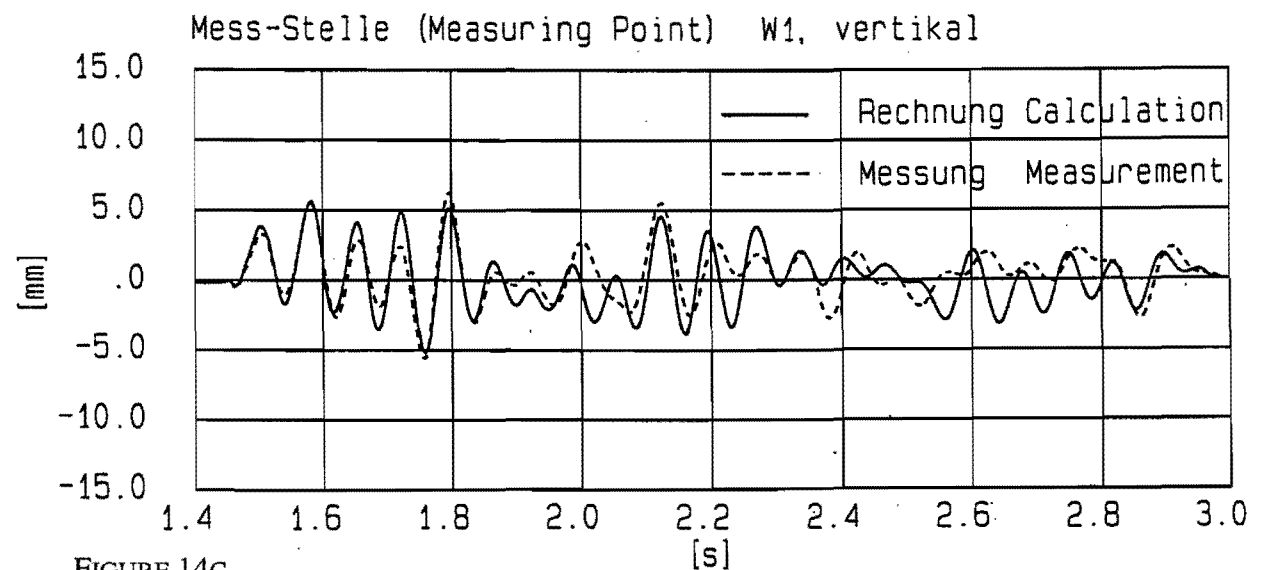
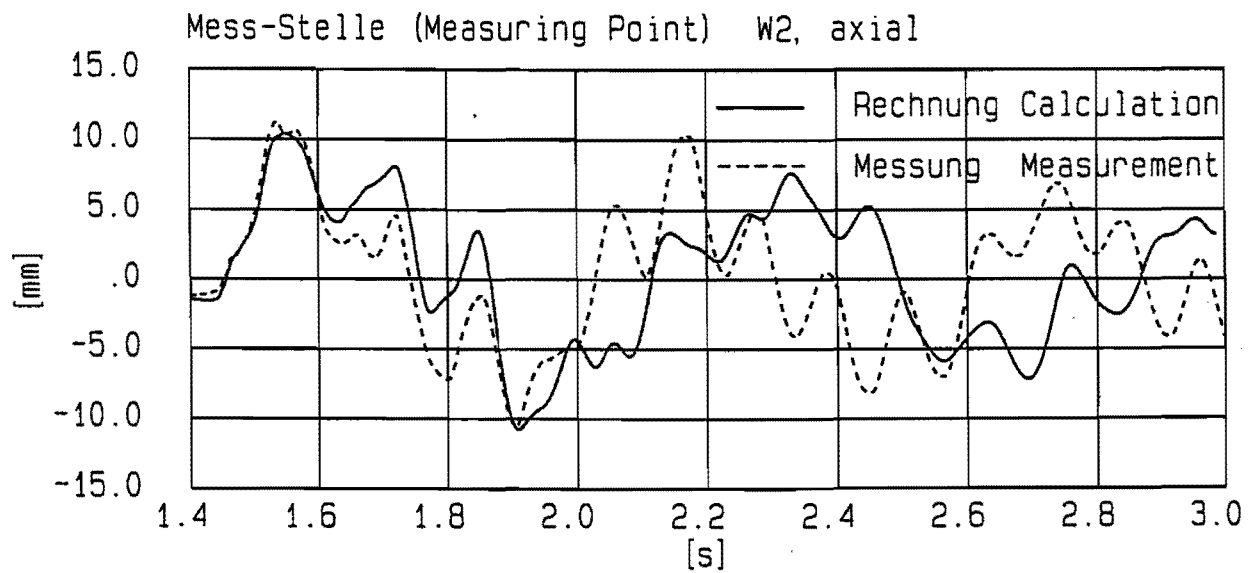
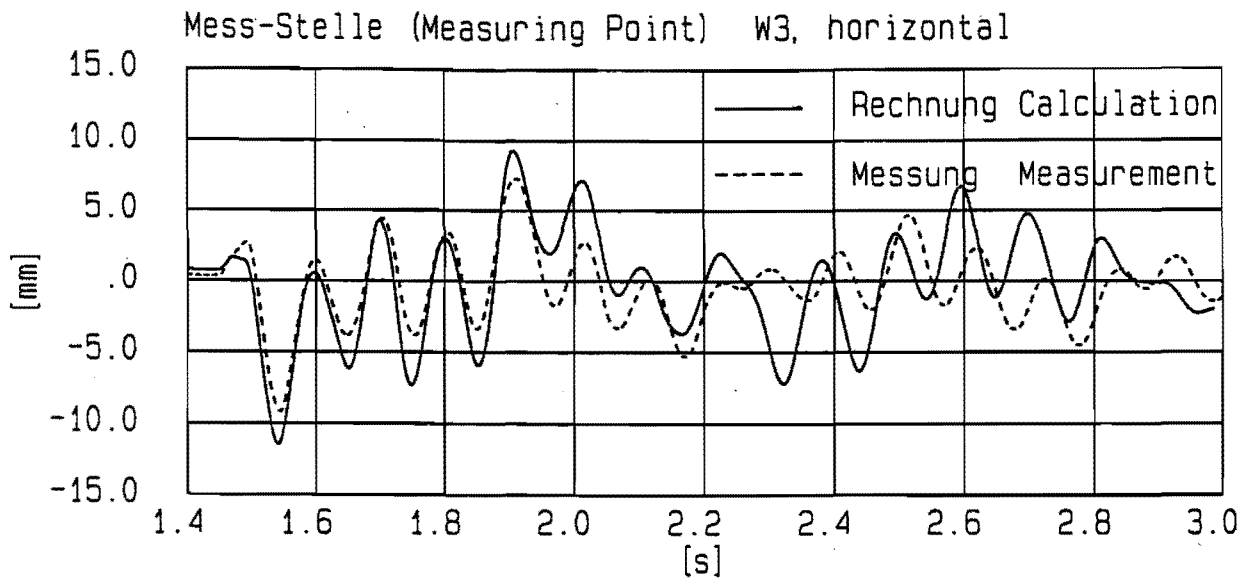


FIGURE 14C.

Pump shutdown with valve closure in nuclear piping system: comparisons between calculation (solid line) and measurement (broken line): displacements [Erath et al, 38].

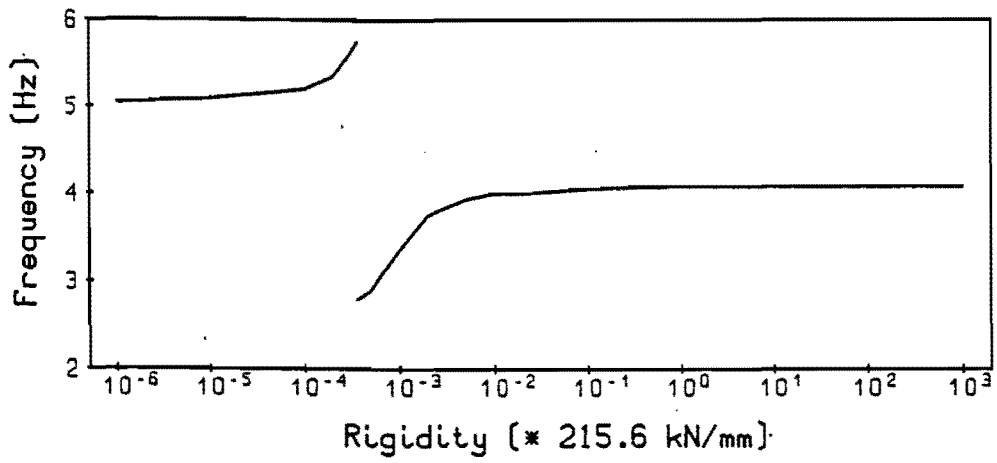
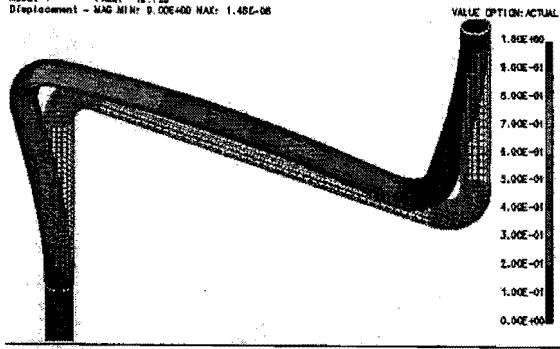


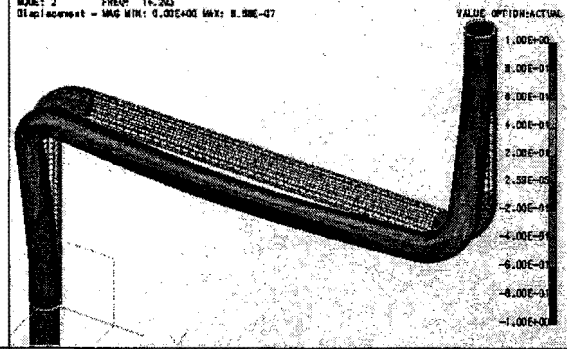
FIGURE 15.

Instantaneous closure of valve in reservoir-pipe-valve-system: main frequency of pressure wave versus rigidity of bend supports [Heinsbroek and Tijsseling, 43].

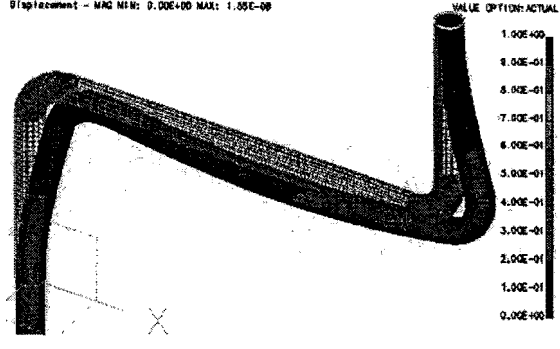
ASTER 5.02.00 CONCEPT MODES CALCULE - CHAMP AUX NOEUDS DE NOM SYMBOLIQUE
 RESULTS: 2-B.C. 0,MODE 1, HYDRO PRESS_2
 MODE: 1 FREQ: 12.723
 Hydro Press - MAG MIN: 0.00E+00 MAX: 1.00E+00
 DEFORMATION: 1-B.C. 0,MODE 1, DISPLACEMENT_1
 MODE: 1 FREQ: 12.723
 Displacement - MAG MIN: 0.00E+00 MAX: 1.45E-08



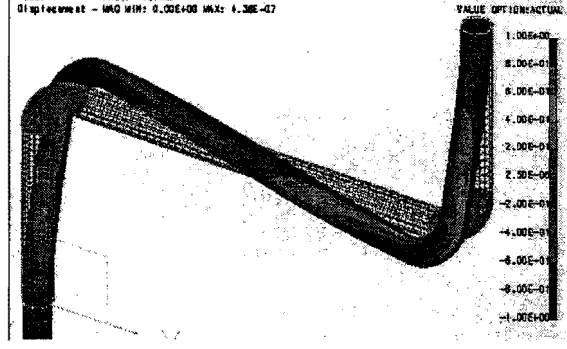
ASTER 5.02.00 CONCEPT MODES CALCULE - CHAMP AUX NOEUDS DE NOM SYMBOLIQUE
 RESULTS: 4-B.C. 0,MODE 2, HYDRO PRESS_5
 MODE: 2 FREQ: 14.203
 Hydro Press - MAG MIN:-1.00E+00 MAX: 1.00E+00
 DEFORMATION: 4-B.C. 0,MODE 2, DISPLACEMENT_4
 MODE: 2 FREQ: 14.203
 Displacement - MAG MIN: 0.00E+00 MAX: 8.59E-07



ASTER 5.02.00 CONCEPT MODES CALCULE - CHAMP AUX NOEUDS DE NOM SYMBOLIQUE
 RESULTS: 6-B.C. 0,MODE 3, HYDRO PRESS_8
 MODE: 3 FREQ: 16.09
 Hydro Press - MAG MIN: 0.00E+00 MAX: 1.00E+00
 DEFORMATION: 7-B.C. 0,MODE 3, DISPLACEMENT_7
 MODE: 3 FREQ: 16.09
 Displacement - MAG MIN: 0.00E+00 MAX: 1.00E-08



ASTER 5.02.00 CONCEPT MODES CALCULE - CHAMP AUX NOEUDS DE NOM SYMBOLIQUE
 RESULTS: 11-B.C. 0,MODE 4, HYDRO PRESS_11
 MODE: 4 FREQ: 20.903
 Hydro Press - MAG MIN:-1.00E+00 MAX: 1.00E+00
 DEFORMATION: 10-B.C. 0,MODE 4, DISPLACEMENT_10
 MODE: 4 FREQ: 20.903
 Displacement - MAG MIN: 0.00E+00 MAX: 4.36E-07



ASTER 5.02.00 CONCEPT MODES CALCULE - CHAMP AUX NOEUDS DE NOM SYMBOLIQUE
 RESULTS: 14-B.C. 0,MODE 5, HYDRO PRESS_14
 MODE: 5 FREQ: 25.559
 Hydro Press - MAG MIN:-0.78E-01 MAX: 1.00E+00
 DEFORMATION: 13-B.C. 0,MODE 5, DISPLACEMENT_13
 MODE: 5 FREQ: 25.559
 Displacement - MAG MIN: 0.00E+00 MAX: 2.88E-08

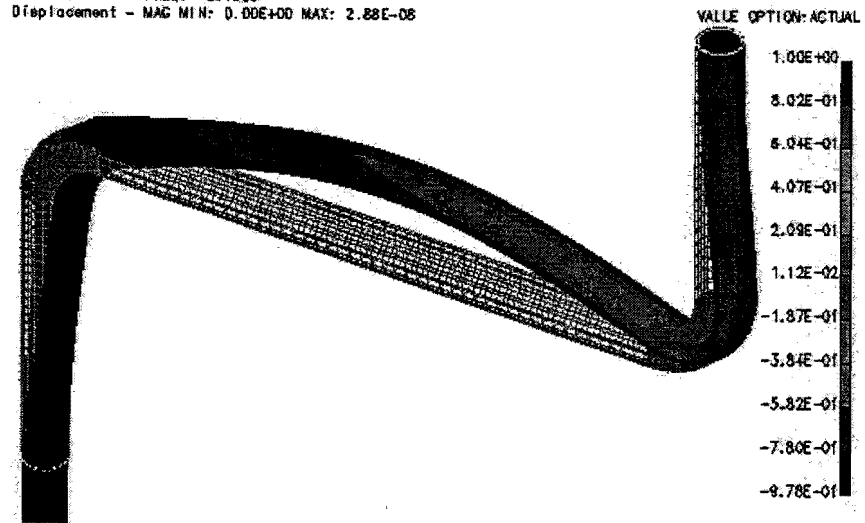


FIGURE 16.

Vibration of a Z-shaped pipe section: prediction showing fully coupled modes [Moussou et al, 56].

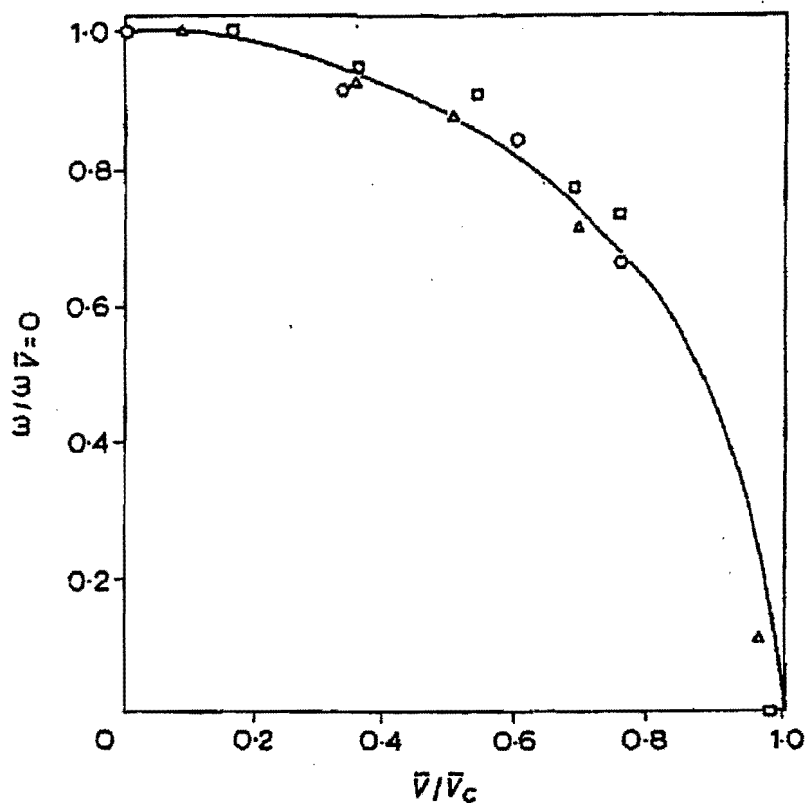


FIGURE 17.

Evolution of the lowest natural frequency of lateral vibration of simply supported straight pipe: (straight line) theory, (symbols) experiment, where $\omega_{\bar{V}=0}$ is the natural frequency corresponding to $\bar{V} = 0$, and \bar{V}_c is the critical velocity. The symbols \circ and \square refer to experiment and the symbol \triangle refers to numerical results [Piet-Lahanier and Ohayon, 88].

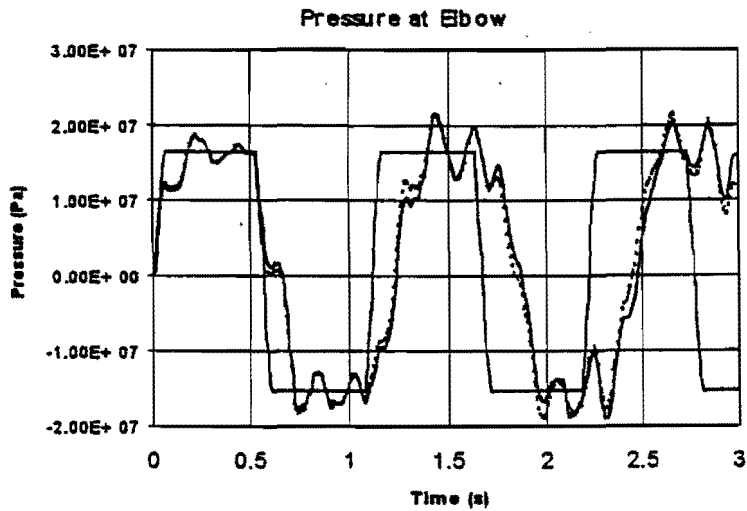


FIGURE 18.

Instantaneous closure of valve in reservoir-pipe-valve-system: prediction of dynamic pressure at elbow; (square wave) no FSI, (solid line) with FSI including centrifugal and Coriolis effects, (dashed line) with FSI only [Wang and Tan, 96].

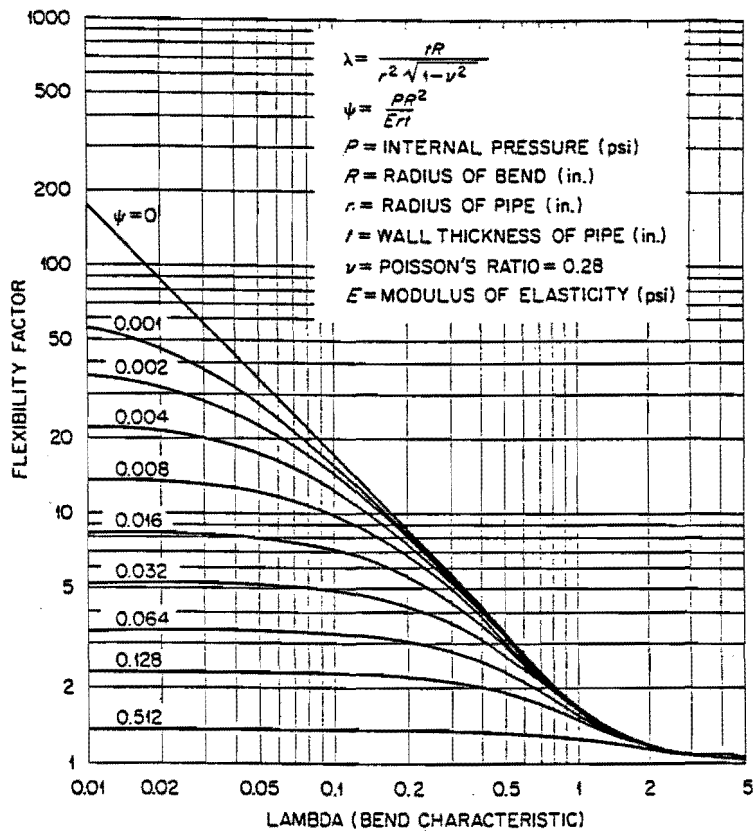


FIGURE 19.

Flexibility factors for elbows as a function of the bend characteristic λ and the internal pressure parameter ψ [Dodge and Moore, 107].

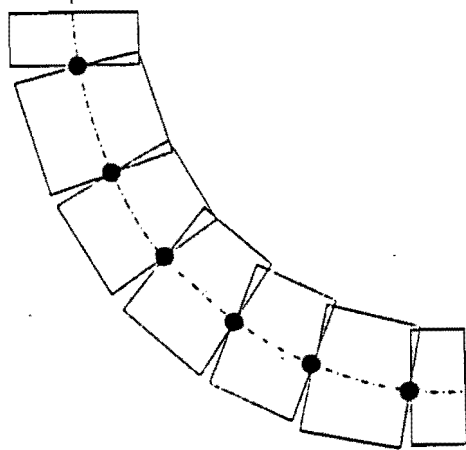


FIGURE 20.

Discrete model of uniformly curved pipe [De Jong, 20].

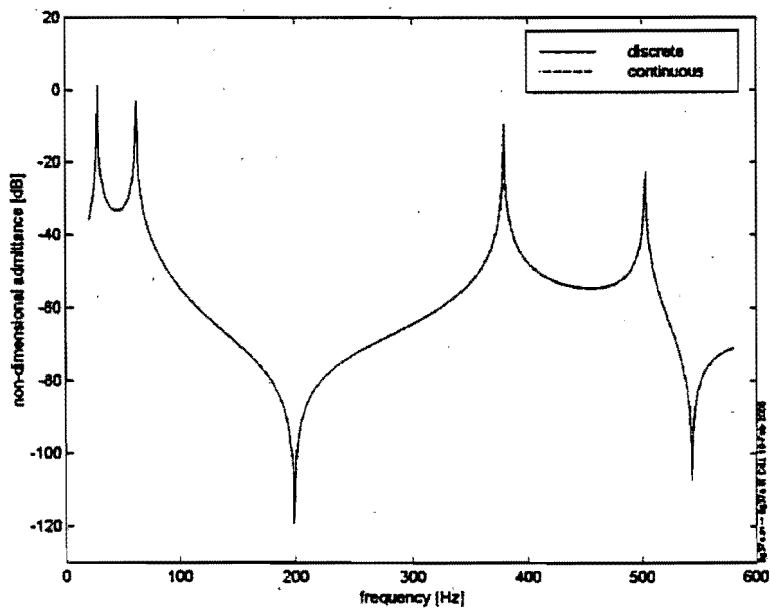
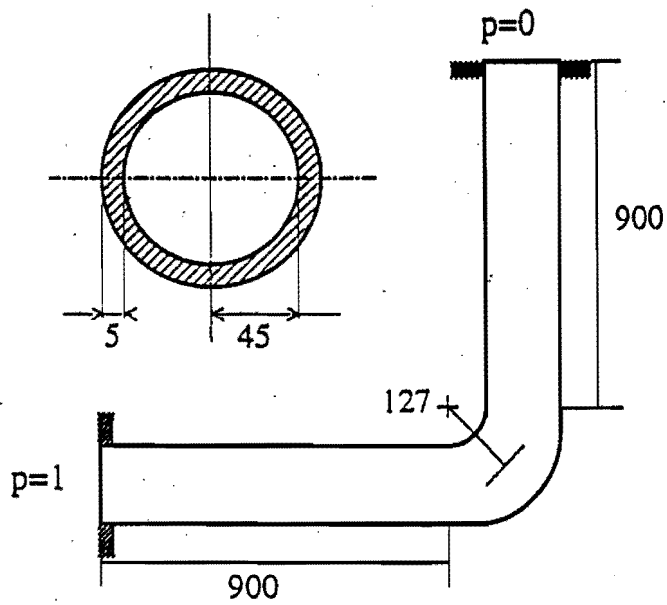


FIGURE 21.

Pipe-elbow system: (upper) pipe-elbow system geometry (dimensions are in mm); (lower) admittance spectrum for two models [De Jong, from errata, 20].

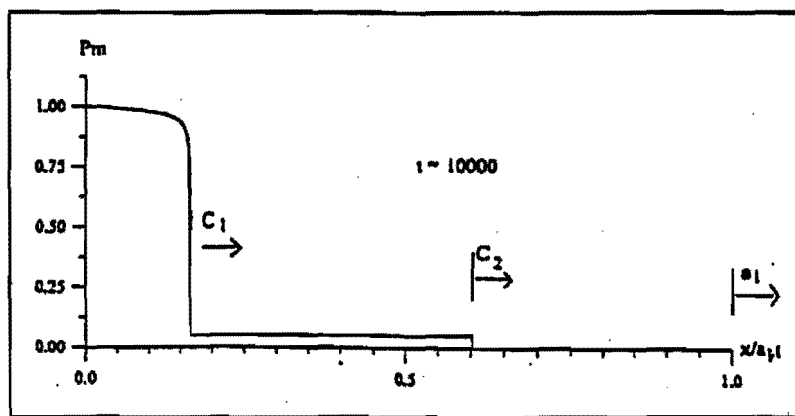


FIGURE 22.

Predicted pressure wave form in the conduit showing the main waterhammer wave traveling at speed c_1 accompanied by the precursor wave traveling at speed c_2 [Bahrar et al, 122].

Theoretical frequencies	Computed (Finite elements) frequencies						
	$\bar{V} = 0$ m/s	$\bar{V} = 0$ m/s	$\bar{V} = 10$ m/s	$\bar{V} = 50$ m/s	$\bar{V} = 70$ m/s	$\bar{V} = 100$ m/s	$\bar{V} = 140$ m/s
23.79	23.78	23.72	22.14	20.49	17.56	1.92	
95.20	95.13	95.09	93.95	92.80			
214.26	214.05	214.01	212.99	211.96			
380.80	380.55	380.51	379.54	378.57			
595.31	594.65	594.61	593.67	592.73			

TABLE 1.

Natural frequencies (in Hz) of lateral vibration of simply supported straight pipe; influence of flow velocity [Piet-Lahanier and Ohayon, 88].

	f_1 [Hz]	f_2 [Hz]	f_3 [Hz]	f_4 [Hz]
FEM model	28	65	387	506
TMM continuous	28	62	<u>378</u>	<u>503</u>
TMM discrete	28	<u>62</u>	<u>379</u>	<u>502</u>

TABLE 2.

Resonance frequencies of pipe-elbow system for three models [De Jong, from errata, 20].